

Integrated Master in Chemical Engineering

***Xylene Isomerization Studies over Acid Catalysts
in the Liquid Phase***

Master's Dissertation

by

Marcelo Filipe Teles de Oliveira

Developed for the dissertation course unit

at

**LSRE-LCM (Laboratory of Separation and Reaction Engineering and Laboratory of
Catalysis and Materials)**



ASSOCIATE LABORATORY

LABORATORY OF SEPARATION AND REACTION ENGINEERING

LABORATORY OF CATALYSIS AND MATERIALS

Supervisor: Dr. Jonathan Gonçalves

Co-Supervisor: Dr. Alexandre Ferreira

Co-Supervisor: Prof. Alírio Egídio Rodrigues



Chemical Engineering Department

July 2019

Agradecimentos

Queria agradecer ao Doutor Jonathan Gonçalves pela constante orientação e contínua disponibilidade em tirar-me todas as dúvidas com o conhecimento que foi adquirindo ao longo destes anos nesta área. Um obrigado também pela ajuda dada na parte experimental, especialmente na atividade de grande esforço físico que era a mudança e empacotamento de algumas colunas, como também pelos vários pontos tirados durante estes extensos tempos de reação.

Desde as aulas de PEQ III e especialmente durante a dissertação, é necessário agradecer ao Professor Alexandre Ferreira por me ter dado esta oportunidade e por me ter mostrado a atitude pragmática que se deve ter dentro de um laboratório, como também a atitude de iniciativa de resolução de problemas, mesmo quando tudo parece estar a afastar-se do plano inicial.

Um agradecimento especial ao Professor Alírio Egídio Rodrigues por ter fornecido o espaço e acesso ao equipamento necessário para executar todos os trabalhos necessários para a conclusão desta dissertação. Também não ficaria sem agradecer à Doutora Cláudia Silva por ter efetuado o teste de caracterização de TPD-NH₃ das amostras de MFI.

A tese, mais que uma disciplina equivalente a 30 ECTS, é o culminar de um curso e de uma experiência de cinco anos que teve profundas mudanças em mim, quer a nível académico quer pessoal. Só faz sentido passar este tempo bem acompanhado, por isso queria agradecer aos membros do NEEQ, à comissão organizadora do VII ENEEQ, e especialmente a vocês: Luísa, Daniel, Ricardo, Sara, Zé, Vilares, Sara Ribeiro e Emanuel pela amizade e ensinamentos dados.

Obviamente, tenho de agradecer à minha pequena grande razão de tudo: a minha família, a minha mãe, o meu pai, o meu irmão e os meus cães, por terem possibilitado que eu experienciasse toda esta magnífica experiência e por serem o meu porto seguro.

Por fim e não menos importante, queria agradecer a todos do LSRE, especialmente à Rute, ao Paulo, à Ana e ao Rafael pela companhia dada e particularmente à Albertina por todos os bolos que trazia para toda a gente (que para além de calorias extras, motivava-nos a relaxar, para depois voltar ao trabalho).

Financiado pelos projetos: NORTE-01-0145-FEDER-000006 - financiado pelo NORTE2020 através do PT2020 e FEDER; Laboratório Associado LSRE-LCM - UID/EQU/50020/2019 - financiado por fundos nacionais através da FCT/MCTES (PIDDAC)

Resumo

A produção de compostos aromáticos tem bastante interesse industrial, sendo que o mercado dos xilenos não é exceção. Esta é uma família de compostos constituída por três isómeros, a saber: *o*-xileno, *m*-xileno e *p*-xileno, sendo este último o detentor de maior interesse industrial, devido à sua capacidade para produzir polietileno tereftalato, PET.

Ultimamente, tem aumentado o interesse em efetuar esta reação através da catálise ácida heterogénea, mas em fase líquida, ao contrário da tradicional reação em fase gasosa, não obstante, também a integração processual que resulta no reator de leito móvel simulado (SMBR) tem incentivado a investigação nesta área.

Neste trabalho, procedeu-se à comparação de catalisadores ácidos com diferentes estruturas e tamanho de poros: MFI, catalisador de tamanho médio, BEA e MOR, ambos catalisadores de poro largo, avaliando-se também o efeito de diferentes razões de $\text{SiO}_2/\text{Al}_2\text{O}_3$. Esta comparação foi efetuada através da reação de *m*-xileno em colunas de leito fixo, em condições operatórias de 513 K, 2,1 MPa e um caudal de $3 \text{ mL}\cdot\text{min}^{-1}$, adicionalmente também se avaliou o comportamento de compostos como tolueno e *p*-dietilbenzeno (PDEB), no sentido de perceber se poderiam ser usados como desorventes num possível SMBR.

Apesar da elevada seletividade dos catalisadores de tamanho médio para o *p*-xileno, os catalisadores de poro largo conseguem obter elevadas conversões, sendo que o MOR-40 obteve a maior conversão, 45,3 %, logo é o melhor candidato para ser implementado num SMBR. O tolueno foi escolhido como desorvente, sendo que o PDEB mostrou uma elevadíssima reatividade para as condições mencionadas.

Palavras Chave (Tema): xilenos, isomerização, catálise ácida, MFI, MOR, BEA

Abstract

The production of aromatic compounds has high industrial interest, particularly the market for xylenes. This is a family of compounds constituted by three different isomers: *o*-xylene, *m*-xylene, and *p*-xylene, being the latter is the one with the highest industrial interest, because it is a reactant to produce polyethylene terephthalate, PET.

Recently, the interest on performing this reaction in heterogeneous acid catalysis and in the liquid phase is increasing, in contrast of the classic gas phase reaction. Additionally, a possible application of a simulated moving bed reactor (SMBR) has also encouraged many researches on this area.

In this work, it was compared acid catalysts with different structures and pore sizes: MFI, medium-pore catalyst, BEA and MOR, large-pore catalysts. It was also evaluated the effect of different SiO₂/Al₂O₃ ratios. To analyze all catalysts, *m*-xylene isomerization was performed in fixed-bed columns at 513 K, 2.1 MPa, and a flow rate of 3 mL·min⁻¹; additionally, it was also evaluated the conversion of toluene and *p*-diethylbenzene (PDEB), in order to evaluate if they could be used as a desorbent in an SMBR.

Even if medium-pore catalyst showed high selectivity towards *p*-xylene, large-pore catalysts have higher conversion; indeed, MOR-40 achieved the highest conversion, 45.3 %, and therefore it is the best candidate to be implemented in an SMBR. Toluene was chosen as the best candidate for desorbent, while PDEB showed high reactivity for the mentioned conditions.

Key words (Theme): Xylene, isomerization, acid catalysis, MFI, MOR, BEA

Declaração

Declara, sob compromisso de honra, que este trabalho é original e que todas as contribuições não originais foram devidamente referenciadas com identificação da fonte.

Porto, 1 de julho de 2019

A handwritten signature in blue ink that reads "Marcelo Filipe Teles de Oliveira". The signature is written in a cursive style and is centered on the page.

(Marcelo Filipe Teles de Oliveira)

Index

1	Introduction.....	1
1.1	Framing and presentation of the work	1
1.2	Outline	2
2	Context and State of the Art	3
2.1	Xylenes.....	3
2.2	Manufacture of Xylenes.....	4
2.2.1	Xylene Production.....	4
2.2.2	PX Separation	4
2.2.3	Process Integration of both Reaction and Separation	5
2.2.4	Isomerization Reaction.....	6
2.2.5	Acid catalysis and Zeolites	10
3	Material and Methods	15
3.1	Choice of xylene reactant.....	15
3.2	Choice of Catalyst.....	15
3.3	Catalyst Shaping.....	16
3.4	Catalyst Characterization	18
3.4.1	Textural Characterization	18
3.4.2	Acid Sites Characterization.....	19
3.5	Experimental Setup and Procedure	19
4	Results and Discussion	23
4.1	Textural Characterization.....	23
4.2	Acid Sites Characterization	29
4.3	Column Characterization	30
4.4	Reaction Results.....	31
4.4.1	Xylene Isomerization	31
4.4.2	Ethylbenzene and toluene.....	35
4.4.3	<i>P</i> -diethylbenzene (PDEB) Isomerization.....	36

5	Conclusions	39
6	Assessment of the work done	41
6.1	Objectives Achieved.....	41
6.2	Limitations and Future Work	41
6.3	Final Assessment.....	43
7	References	45
	Appendix A - Regeneration Program	49
	Appendix B - Chromatographs.....	50
	Appendix C - SEM	51
	Appendix D - Mass transfer resistances.....	56
	External Mass Resistance	56
	Internal Mass resistances	58
	Compound properties	60
	Appendix E - EB/Tol Experiments.....	63
	Appendix References	65

Notation and Glossary

A_p	Particle area	cm^2
D_{AA}	Molecular diffusivity as self-diffusivity	$\text{cm}^2 \cdot \text{s}^{-1}$
D_e	Effective Diffusivity	$\text{cm}^2 \cdot \text{s}^{-1}$
$D_{i,m}$	Molecular diffusivity for mixtures calculated by Wike-Chang equation	$\text{cm}^2 \cdot \text{s}^{-1}$
D_m	Molecular diffusivity	$\text{cm}^2 \cdot \text{s}^{-1}$
R_{obs}	Observed reaction rate	$\text{mol} \cdot \text{g}_{\text{cat}}^{-1} \cdot \text{s}^{-1}$
T_c	Critical temperature	K
V_c	Critical molar volume	$\text{cm}^3 \cdot \text{mol}^{-1}$
V_p	Particle volume	cm^3
d_p	Particle diameter	cm
k_f	Liquid phase mass transport coefficient	$\text{cm}^2 \cdot \text{s}^{-1}$
V	Liquid molar volume	$\text{cm}^3 \cdot \text{mol}^{-1}$
v	Superficial Velocity	$\text{cm} \cdot \text{s}^{-1}$
x	Molar fraction	
X	Reactant conversion in mole basis	
C	Molar concentration	$\text{mol} \cdot \text{dm}^{-3}$
Ca	Carberry number	
I	Bessel function	
K	Boltzmann constant	$\text{m}^2 \cdot \text{kg} \cdot \text{s}^{-2} \cdot \text{K}^{-1}$
L	Column height	cm
M	Molar mass	$\text{g} \cdot \text{mol}^{-1}$
N	Avogadro number	mol^{-1}
Q	Flow rate	$\text{mL} \cdot \text{min}^{-1}$
Re	Reynolds number	
Sh	Sherwood number	
Sc	Schmidt number	
T	Absolute temperature	K
W	Mass of dry catalyst	g

Greek letters

ε	Bed porosity	
ε_p	Particle porosity	
ρ_p	Particle apparent density	$\text{g} \cdot \text{cm}^{-3}$
μ	Dynamic viscosity	cP
Φ	Association coefficient	
η	Effectiveness factor	
ω	Acentric factor	
ϕ	Thieles modulus	

Indices

i	Component
-----	-----------

List of Acronyms

BEA	Structure code for zeolite beta
Bz	Benzene
DEB	Diethylbenzene
EB	Ethylbenzene
EDS	Energy dispersive spectroscopy
FID	Flame Ionization detector
FTIR	Fourier-transform infrared spectroscopy
GC	Gas chromatography
MFI	Structure code for zeolite ZSM-5
MOR	Structure code for zeolite mordenite
MX	<i>m</i> -xylene
OX	<i>o</i> -xylene
PDEB	<i>p</i> -diethylbenzene
PET	Polyethylene terephthalate
PX	<i>p</i> -xylene
SEM	Scanning electron microscope
SMB	Simulated moving bed
SMBR	Simulated moving bed reactor
TEB	Triethylbenzene
TMB	Trimethylbenzene
TNT	2,4,6-Trinitrotoluene
Tol	Toluene
TPD	Temperature programmed desorption
XRD	X-ray diffraction
ZSM-5	Zeolite Socony Mobil number 5

1 Introduction

1.1 Framing and presentation of the work

Xylenes are one of the most important aromatic compounds. Although, there are three different isomers, namely *o*-xylene (OX), *m*-xylene (MX) and *p*-xylene (PX), the last one is by far the most desired, because it is the main reactant to produce polyethylene terephthalate (PET), which is used as polyester fiber, resin, and films [1].

In fact, polyester was the most used synthetic fiber worldwide in 2014 and the global *p*-xylene market is expected to grow up to 81.02 billion USD by 2022, which goes according with the rise in demand for PET containers [2].

Manufacture of xylenes is divided in three steps: production of mixed xylenes, followed by separation of PX, which is commonly made by crystallization or adsorption and finally an acid catalyzed isomerization reaction of mixed xylenes with low concentration of PX, in order to reestablish the chemical equilibrium and maximize the production of PX by transformation of the other isomers [3].

Shape-selective catalysts have been object of study for two reasons, all isomers have similar physical properties, so separation is a troublesome task, and mainly because 83.4% of the cost of PX production is related with naphtha feedstock, therefore the producer with improved product selectivity will have fair advantage in the market [4, 5].

Conversely, intensification of processes has attracted attention due to reduced investments, less energy and operating costs. In this case, Simulated Moving Bed Reactor (SMBR) has been proposed to produce PX, allowing one to overcome the chemical equilibrium inherent to the isomerization reaction. Although the isomerization of xylenes is industrially conducted in the gas phase, in the SMBR it is done in the liquid phase with the disadvantage of not being able to transform ethylbenzene, but with the benefit of less energy consumption and prolonged catalyst life, because the coke precursors are dissolved in the liquid and taken out of the reactor [3]. For this isomerization reaction, catalyst selectivity and activity are influenced mainly by parameters such as pore dimensions and architecture and acidity.

In this work, it was evaluated six zeolites with different pore architecture and SiO₂/Al₂O₃ ratio and therefore different acidity: MFI-25, MFI-30, MFI-38, MOR-20, MOR-40, and BEA-35, where the numeric suffix denotes for the corresponding SiO₂/Al₂O₃ ratio. The study was carried out through fixed-bed experiments in the liquid phase at 513 K, 2.1 MPa in order to study *m*-xylene conversion, catalyst selectivity towards *p*-xylene, and formation of secondary products.

1.2 Outline

This work has seven chapters: Introduction, Context and State of the Art, Material and Methods, Results and Discussion, Conclusions, Assessment of the work done, and References.

In chapter 1, Introduction, there is a brief description of what motivated this work.

Context and state of art presents the most fundamental theoretical aspects related with xylenes, acid catalysis, and zeolite catalysts.

Chapter 3, Materials and Methods, has the information containing the pure xylene reactant chosen to perform isomerization reaction, description of the catalysts used and the corresponding shaping process, and the experimental setup and procedure.

Chapter 4, Results and Discussion, contains the collection of all characterization and reaction results with interpretation and discussion on how a catalyst performed based on their physical and chemical characteristics.

Chapter 5, Conclusion, covers the most important conclusions of this thesis based on the discussion above.

Chapter 6 is a retro evaluation of all work done and future work, while all references used in this work are in Chapter 7.

Finally, Appendix A, B, C, D and E serve as support information to this work.

2 Context and State of the Art

2.1 Xylenes

Xylenes are aromatic compounds that have the molecular formula C_8H_{10} . They are composed by a benzene ring with two methyl groups attached, hence there are three xylene isomers, *o*-xylene (OX), *m*-xylene (MX) and *p*-xylene (PX), as shown in Figure 1.

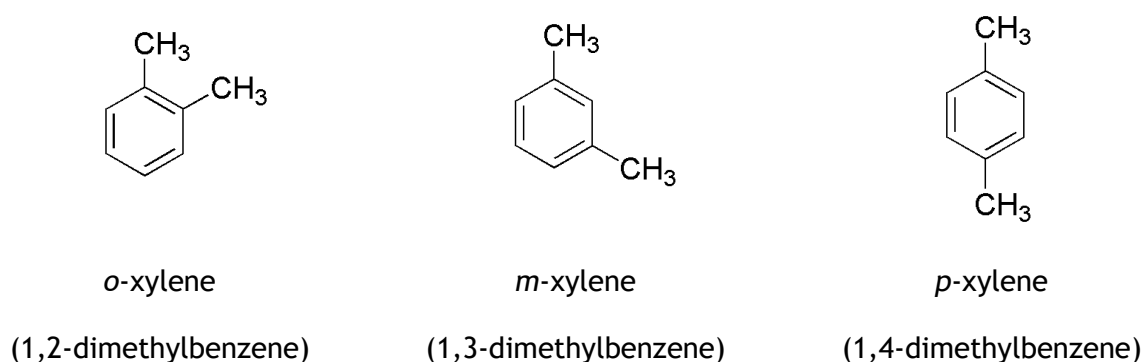


Figure 1. Xylene isomers.

It is important to understand that ethylbenzene (EB) has the same molecular formula as any other xylene, but it is not considered one. Generally, most of the industrial streams have a near-equilibrium composition between xylenes and ethylbenzene, and one should use the term “mixed xylenes” to describe such mixture [1].

PX is by far the isomer with higher industrial interest, it is the raw material to synthesize terephthalic acid, the main reactant to produce polyethylene terephthalate (PET) which is used as polyester fiber, resin, and film. Additionally, the investment in solar cells is increasing and PET is one of the main compounds that is used to produce flexible polymer substrates, which improves the integration of solar cells with other devices [6].

The second most important isomer is OX, which is used to produce phthalic anhydride in order to synthesize plasticizers and alkyd resins. Unfortunately, even though it is the majority compound in the chemical equilibrium, MX is the less important, being used to produce isophthalic acid and isophthalonitrile [1].

PX accounts for 80 % of the global xylene consumption, while OX and MX represent 12 % and 3 %, respectively. Leaving 5 % for the use of mixed xylenes as solvent [1]. Cost wise, MX is the most expensive, while OX is the cheapest [7].

2.2 Manufacture of Xylenes

The industrial manufacture of xylenes is comprised by the following three steps: production of mixed xylenes, separation of the higher value isomers (PX and/or OX) and finally isomerization to reestablish the chemical equilibrium and hence maximizing the quantity of PX, as shown in Figure 2 [3].

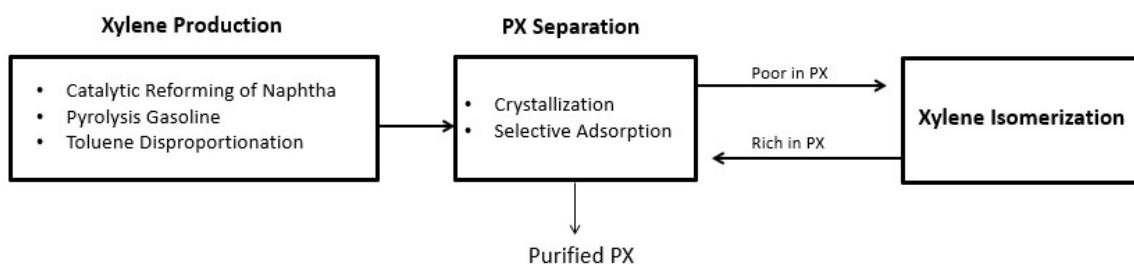


Figure 2. Simplified aromatics complex diagram.

2.2.1 Xylene Production

There are three ways to produce mixed xylenes: catalytic reforming of naphtha, pyrolysis gasoline, and disproportionation of toluene [8]. Additionally, the latter can be applied together with transalkylation of toluene with heavy aromatics [9].

Catalytic reforming of naphtha is the most common way to produce xylenes, accounting for 70 % of their production [1]. The purpose of this process is to increase the number of octanes in the mixture by transforming straight chained paraffins and cyclic aliphatic hydrocarbons into branched paraffins and aromatics, respectively. Catalytic reforming is operated under high temperature (723-793 K) and pressures ranging 4 to 30 bar, resulting in a product rich in aromatics such as benzene, toluene, xylenes, and ethylbenzene [10].

Toluene (Tol) application is limited to production of trinitrotoluene (TNT) or as a solvent to produce paints; however, it can be transformed into higher value products such as benzene and xylenes by disproportionation. This process is not as economical as catalytic reforming of naphtha, but it is a strategy that could be adapted to produce more xylenes, when the market demands so [11].

2.2.2 PX Separation

Xylenes have very similar molecular structures, therefore their physical properties do not differ significantly, as seen in Table 1. Due to this fact, separation is a very troublesome task. OX can be separated by distillation, but it is practically impossible to separate PX and MX with this method, because of their close boiling points [12].

To separate PX, crystallization or selective adsorption are the preferred methods. The former is related with the higher freezing point of PX, allowing it to concentrate in the solid phase, and the latter is related to the affinity between PX and a particular adsorbent, which depends on its molecular structure [13].

PX recovery by crystallization is limited to 60-70% due to eutectic constraints in equilibrium mixtures of xylenes and has high energy requirement to operate at low temperatures [3].

Table 1. Xylene isomers' physical properties.

	OX	MX	PX
Boiling Point (K) [12, 14]	417.6	412.3	411.5
Freezing Point (K) [12]	248.0	222.5	286.5
Minimum Cross Diameter [15]	7.25	7.27	6.63

The preferred technology to separate PX depends on the composition of the feedstock, if it is rich in PX, above 80%, crystallization methods are favored; otherwise selective adsorption is the best option and indeed it is the dominant method in the industry accounting for 75 % of the PX production. The most employed technologies are UOP's Parex, Toray's Aromax, and IFP's Eluxyl with PX recovery of 97-99 % and purity of 99,7 - 99,9% [12].

2.2.3 Process Integration of both Reaction and Separation

SMBR has been proposed as a safer, more sustainable, and cheaper alternative route to produce xylenes. This equipment is a multifunctional reactor, where product separation occurs in the same unit. Process intensification of both reaction and separation has many advantages: reduced equipment size, reduced production-capacity ratio and lower consumption of energy [16].

As the name states, SMBR is an extension of SMB, which is already used for PX separation, but in this case the columns that constitute it are filled with both catalysts and adsorbent. Both technologies are based on the True Moving Bed (TMB), where the movement of the liquid phase (containing the reactants) and the adsorbent/catalyst is made in countercurrent, but due to the practical limitations to perform this type of movement, the countercurrent flow is simulated by a synchronous shift by one column of the two inlet streams (feed and desorbent) and the two outlet streams (extract and raffinate) in direction of the fluid, as seen in Figure 3 [17].

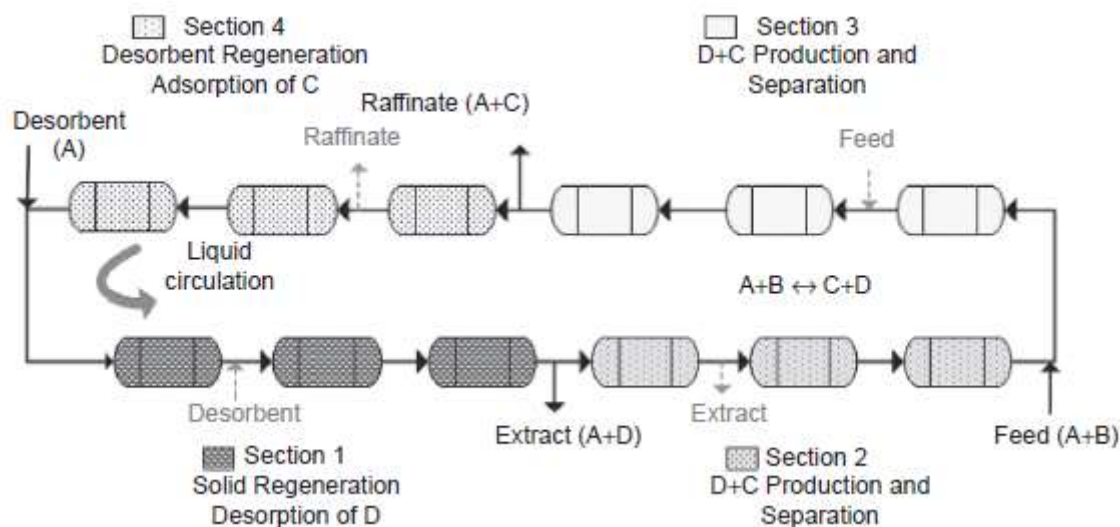


Figure 3. Schematic representation of an SMBR constituted by 3 columns per section, for a reaction of reactant A and B forming the less-adsorbed product C and more-adsorbed product D. Copied from [17].

The four existing streams divide this equipment in four different zones or sections [18]:

- Section 1, where the adsorbent is regenerated by desorption of the more-adsorbed product by using the desorbent.
- Section 2, placed between the extract and feed node, where the reaction products are being formed, wherein the more-adsorbed product is transported with the solid in direction to the extract node, while the less-adsorbed product is transported with the liquid to the raffinate port.
- Section 3, between the feed and raffinate node, same function of section 2.
- Section 4, where the desorbent is regenerated and adsorption of the less-adsorbed product prevents the contamination of the more-adsorbed product in the extract node.

2.2.4 Isomerization Reaction

As seen in Figure 2, after separation, the stream depleted of PX goes to an isomerization unit to reestablish the chemical equilibrium, thus transforming MX and OX into PX. There are two different reaction schemes proposed for xylene isomerization, namely linear scheme and triangular scheme, as shown in Figure 4 [19]. The linear scheme only allows conversion of OX into PX and vice versa, via MX as intermediate, conversely triangular scheme allows direct transformation between any isomer.

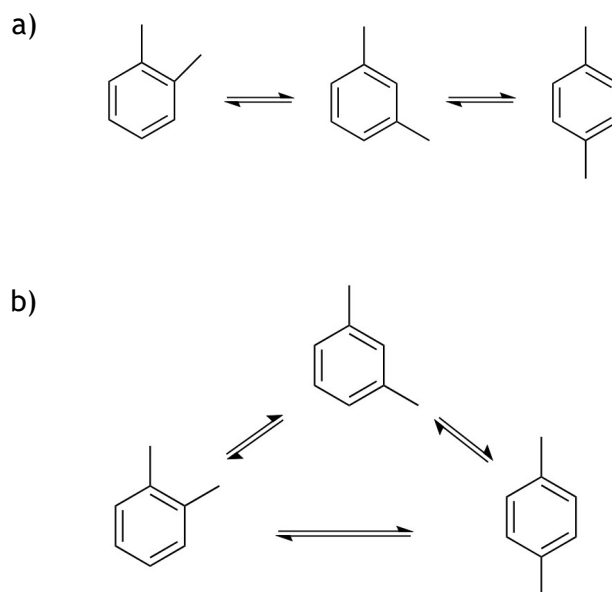


Figure 4. a) Linear scheme, b) triangular scheme.

There are two different mechanisms of reaction. One is the intramolecular or monomolecular mechanism, where all changes happen in the same molecule through a 1,2-methyl shift on the benzenium ion resulting from protonation by an acid site, as seen in Figure 5. The other is the intermolecular or bimolecular mechanism, where two xylenes react with each other initially by disproportionation and then by transalkylation, Figure 6.

Clearly, 1,2-methyl shift is the mechanism present in the linear scheme, where, for example, OX transforms into PX by continuous 1,2-methyl shifts and MX acts as an intermediate. For the triangular scheme, transformations could happen by either 1,2-methyl shift and 1,3-methyl shift. In this case, the cause of the apparent direct conversion of OX into PX was thought to be done by 1,3-methyl shift but is most likely due to the low diffusivity of MX, which by staying longer inside the catalyst seems that OX is transformed directly into PX [20].

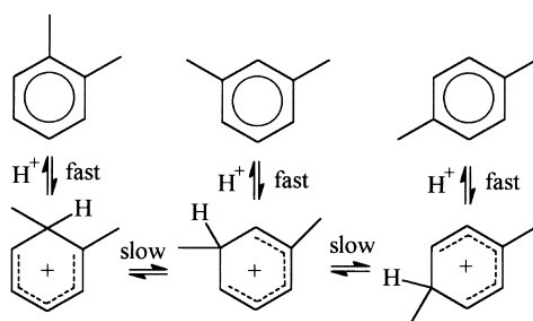


Figure 5. Intramolecular mechanism for xylene isomerization [21]

The intermolecular or bimolecular mechanism, Figure 6, is another possibility, where different xylene molecules react with each other by disproportionation forming trimethylbenzene (TMB) that reacts with other xylenes by transalkylation, changing the position of the methyl group on the benzene ring [21]. The formation of TMB requires a bulky intermediate, tri and tetra methylated diphenylmethane, which is a bigger molecule in comparison to all other molecules previously mentioned; therefore, this mechanism is limited to catalysts with pores big enough to accommodate it [22]. For large-pore catalyst, the direct transformation of OX into PX is due to this mechanism.

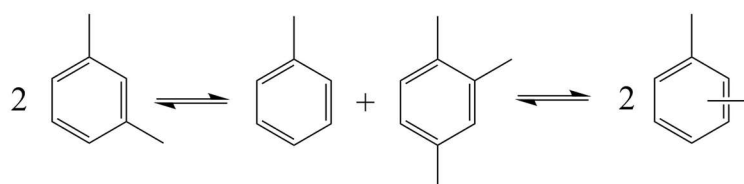


Figure 6. Intermolecular mechanism for xylene isomerization.

There is always a competition between the two mechanisms, but the intramolecular mechanism will prevail for catalysts with steric constraints made by the lower pore size, which do not have enough space to form bulky intermediates, and catalysts with very strong acid sites, while intermolecular mechanism needs larger pores and weaker acid sites [21]. Additionally, the operating conditions also affect the mechanism, being that the contribution of the intermolecular mechanism is favored at lower temperatures, below 470 K, due to its lower activation energy [23].

The intermolecular mechanism has a lower activation energy, but at the same time the bulky intermediate, that is formed, is present in many secondary reactions, therefore higher quantity of secondary products is expected to be present in large-pore catalyst.

Another important detail is the presence of ethylbenzene. As previously mentioned, industrial streams have this compound in their composition, which can trigger multiple side reactions and one should consider if it should be removed, for example for production of PX in an SMBR [3], or taking advantage of it by transforming it into xylenes, using bifunctional EB isomerization catalysts, or transforming it into benzene, using EB dealkylation catalysts [1].

Possible side reactions are xylene disproportionation, EB disproportionation, Tol disproportionation, EB-Tol transalkylation, EB-Xylene transalkylation, EB-Xylene transmethylation which are represented from Figure 7 to Figure 12, respectively. The secondary products of these reactions are: benzene, toluene, diethylbenzenes, ethyltoluenes, ethylxylenes and trimethylbenzenes [24]. Additionally, *p*-diethylbenzene (PDEB) is often used as desorbent in SMB during PX separation, therefore PDEB disproportionation, Figure 13, and

isomerization, Figure 14, were included in the next set of possible reactions related with the subject of xylene isomerization.

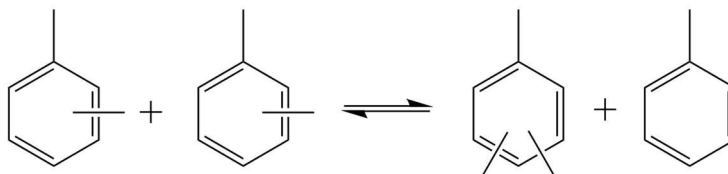


Figure 7. Xylene Disproportionation reaction.

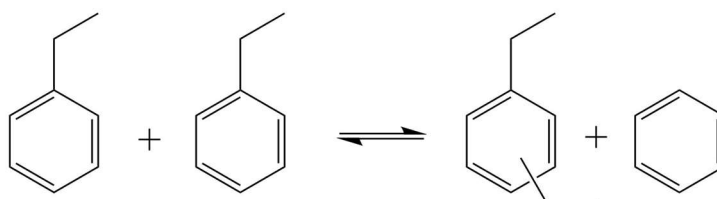


Figure 8. Ethylbenzene Disproportionation reaction.

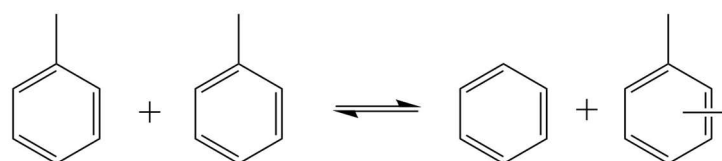


Figure 9. Toluene Disproportionation reaction.

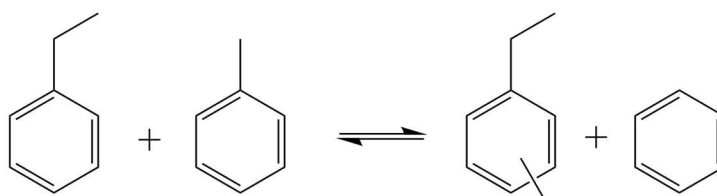


Figure 10. Ethylbenzene - Toluene Transalkylation reaction.

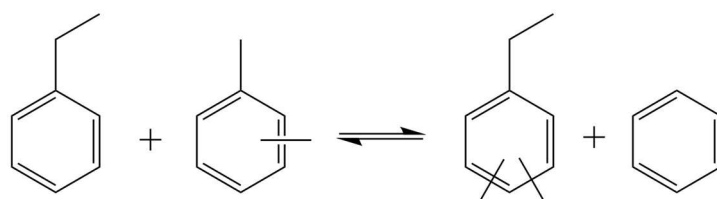


Figure 11. Ethylbenzene - Xylene Transalkylation reaction.

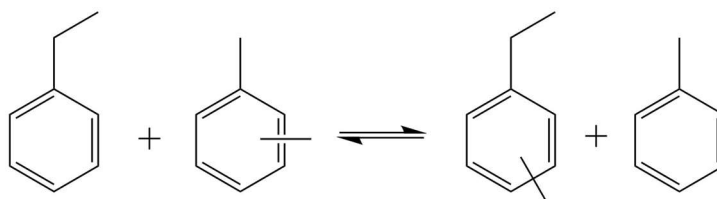


Figure 12. Ethylbenzene - Xylene Transmethylation reaction.

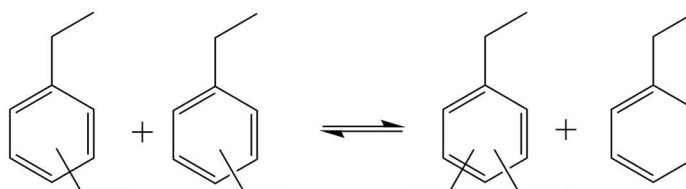


Figure 13. Diethylbenzene Disproportionation reaction.

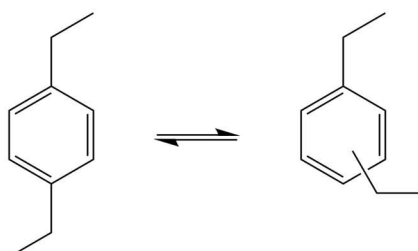


Figure 14. *P*-diethylbenzene isomerization reaction.

2.2.5 Acid catalysis and Zeolites

Because the purely thermal isomerization requires extreme operating conditions and has poor yields, it is necessary to use acid catalyst in either the liquid or gas phase to make this reaction viable in an industrial scale [25].

Different types of catalysts with acidic properties have been experimented. Aluminium chloride and boron fluoride were some of the firsts, but because their high acidity, they were very corrosive and had problems with catalyst regeneration, thus being a poor choice [26].

Acidic halides, such as HF-BF_3 , also known as Friedel Crafts catalysts, were used in the liquid phase and are very active even at low temperatures, but they have problems concerning: deactivation by reaction with water and sulphur in the feed, losses by dissolution in the product, shown poor selectivity and their acidic nature could cause problems in the equipment too [27].

To solve the deactivation and acidity problems, amorphous aluminium silicates were studied, but their acidity based on Al-OH groups is not as strong as zeolites, which have an crystalline structure and acidity based on Si-OH-Al [28]. Thus, zeolites showed the most promising results.

As seen in Figure 15, they are composed by primary building units (PBU) of silicium cations (Si^{4+}) and aluminium cations (Al^{3+}), which are surrounded by four oxygen atoms [29].

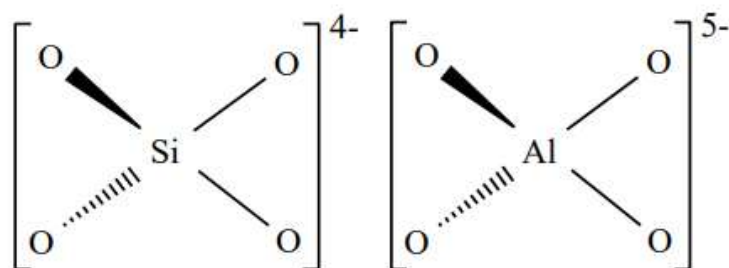


Figure 15. Tetrahedral arrangement of the SiO_4^{4-} and AlO_4^{5-} as the primary building blocks of zeolites [29].

The ratio between silicium (Si) and aluminium (Al) in the zeolite is what makes it acid. Vast majority of its composition is silicium atoms, but when they are substituted by aluminium, there is an extra negative charge that must be counter-balanced by an outside cation, that in some cases is a ammonium cation, which followed by thermal decomposition can generate in this way a Brønsted acid site, a proton [30]. Other ways to form Brønsted acid sites are reduction to a lower valence state of exchanged metal ions and hydrolysis of polyvalent cations [31].

It is important to analyze the type of acid sites that can be found in a zeolite, indeed acid catalysis is mainly influenced by the quantity of Brønsted acids (proton donators); however Lewis acids (electron pair receiver) can increase the strength of the Brønsted acids [31]. Structural defects or extra-framework aluminium generate Lewis acid sites, as seen in Figure 16 [29].

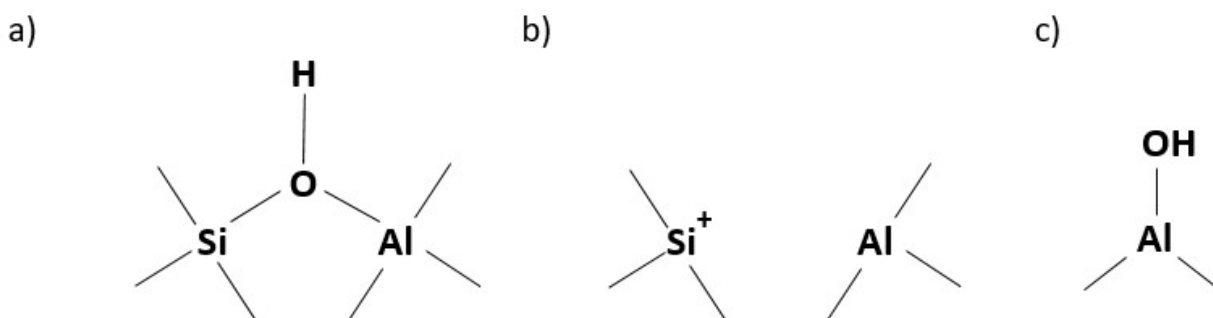


Figure 16. Types of acid sites in zeolites: (a) Brønsted acid site as a bridging OH group, (b) Lewis acid site as a structural defect and (c) Lewis acid site as an extraframework aluminium.

Adapted from [30].

The features that make zeolites a material with so much industrial interest are:

- Structure - vast variety of structure architectures and size of the crystalline rearrangement
- High surface area
- Shape selectivity
- Tuning of chemical properties - the performance of the catalyst can be enhanced by modifying its $\text{SiO}_2/\text{Al}_2\text{O}_3$ ratio [32] or by deactivation of the external acid sites that do not have shape selectivity towards PX [33].

Different product distributions are obtained when using different zeolites, because they have different shape selectivity [34].

MFI-type catalysts have medium pore size and tridimensional pore system of interconnected channels consisting of straight and zig-zag channels. The straight channels are elliptical and have dimensions of 0.53 nm x 0.56 nm, while the zig-zag channels have dimensions of 0.51 nm x 0.55 nm [35].

As seen on Table 1, these dimensions are very close to the PX kinetic diameter, therefore it is expected to have higher product selectivity towards PX over the other isomers. The reduced pore size will create diffusion limitations to molecules that are too bulky to diffuse fast enough and by staying longer at the active acid sites there is a higher probability to be converted into other products [34]. In this case, OX and MX are expected to stay longer in the catalyst pores and therefore being transformed into PX. Additionally, bulky intermediates due to bimolecular reaction mechanisms should not get enough space to form, therefore it is expected the monomolecular mechanism to be the prevalent one in this type of catalyst. MFI-type catalysts find many industrial applications; indeed, ZSM-5 (Zeolite Socony Mobil Number 5) is the main catalyst used in the gas phase isomerization of xylene, which is a MFI-type catalyst [36].

Zeolites mordenite (MOR) and beta (BEA) are large-pore catalysts [30]. Mordenite has a two-dimensional pore system, where the main channel consists of a 12-ring pore of dimensions 0.67 nm x 0.70 nm which is interconnected to smaller pores, 8-ring of dimensions 0.26 nm x 0.57 nm [37, 38]. The 8-ring channels are small enough to prevent diffusion, hence many times mordenite is considered to have a one-dimensional pore system. It has many applications as a catalyst and is used for isomerization, hydrocracking, and production of dimethylamines due to its high thermal and acidic stability [38].

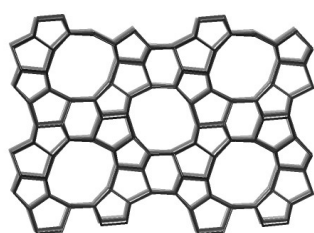
Conversely, beta zeolite catalysts have slightly smaller pores, consisting in a three-dimensional pore system of 12-ring pores to straight channels with a diameter of 0.66 nm x 0.67 nm and sinusoidal channels with a diameter 0.56 nm x 0.56 nm [37]. Industrially, it finds application in ethylbenzene and cumene production [39].

Table 2 presents the most relevant features of these catalysts, while the framework for each of them is represented in Figure 17.

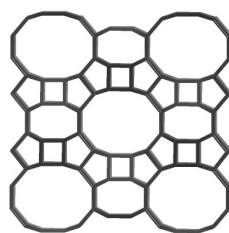
Table 2. Structural characteristics of MFI-, MOR- and BEA-type catalyst

Zeolite Framework type ^a	Ring Size	Channel Dimensionality	Pore Size (nm)
MFI	10	3D	0.51 x 0.55
MOR	12	2D	0.67 x 0.70
BEA	12	3D	0.66 x 0.67

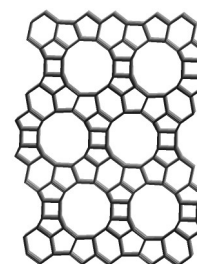
a: nomenclature approved by the Structure Commission of the International Zeolite Association (IZA-SC)



a) MFI



b) MOR



c) BEA

Figure 17. Framework for every catalyst used. Adapted from [40].

Interest on large-pore catalysts is increasing as the popularity of SMBR to perform xylene isomerization in the liquid phase is increasing too. In the liquid phase, the diffusion into the channels is slower than in gas phase and the adsorption processes are more hindered due to lower entropy of the molecules to establish the right angle of orientation [41, 42]. Thus, large-pore catalysts are being more implemented, especially because of their high conversion, which is the main requirement for SMBR applications, since the selectivity towards PX is provided by the adsorbent [42].

3 Material and Methods

3.1 Choice of xylene reactant

To compare all catalysts MX isomerization was proposed, because it represents better the conditions found in the industry. Indeed, MX is the major compound in equilibrium and after separation of PX in units such as Parex, almost no PX is found in the feedstock of the isomerization units. Therefore, MX is always the major compound, especially if naphtha feedstock is sent to a distillation column for pre-separation of OX [1].

Further studies were performed to study secondary reactions in order to understand the influence of molecules like Tol, EB, and PDEB have in the reaction performance. Pure PDEB and 50/50% in mass of Tol and EB experiments were conducted in order to study the viability of Tol and PDEB as desorbent in an SMBR.

In all experiments n-heptane was used as eluent.

High purity MX (>99 %) and high purity EB (>99,8 %) were purchased from Acros Organics™; 100 % assay (GC) Tol was purchased from VWR Chemicals™; high purity n-Heptane (>99 %) was purchased from Honey well Riedel-de Haën™; and finally, PDEB was kindly provided by the Institut Francais du Petrole. The compounds were used without further treatment or purification.

3.2 Choice of Catalyst

MX isomerization was performed in three different types of zeolites (i.e., MFI, MOR, and BEA); within the same structure, it was also study the effect of different SiO₂/Al₂O₃ ratios, as stated in Table 3.

Table 3. Catalysts used.

Catalyst/structure	SiO ₂ /Al ₂ O ₃
MFI	25
	30
	38
MOR	20
	40
BEA	35

Clariant kindly provided shaped MFI-30 catalyst in the acid form, powder MOR-20 in the ammonium form, and powder BEA-35 in the acid form, while Süd Chemie (now part of the Clariant group) kindly provided shaped MOR-40 in the acid form. Powder of the MFI-38 catalyst, in the ammonium form, was purchased from ACS Materials and MFI-25 zeolite powder was kindly provided by other company in the acid form. MFI-25, MFI-38, MOR-20, and BEA-35 materials were further shaped into pellets.

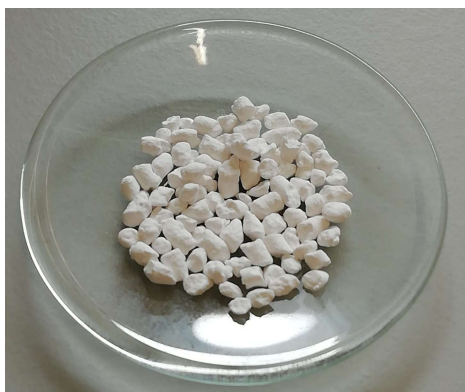
3.3 Catalyst Shaping

MFI-25, MFI-38 and MOR-20 were shaped in Laboratory of Separation and Reaction Engineering (LSRE) at Faculdade de Engenharia da Universidade do Porto (FEUP) using the equipment Caleva Multi Lab, which is a granulator/mixer, extruder and spheronizer in the same equipment. Sample trials were made to obtain the best parameters in order to shape each catalyst. The parameters used were: a mixing velocity of 80 rpm for 15 minutes followed by 5 minutes at 50 rpm, an extrusion velocity of 60 rpm through a perforated die with 2 mm diameter openings, and then a spheronizer velocity sufficiently enough to have a roping-like movement of the pellets, between 300-700 rpm. All catalysts shaped this way have 30% of nanopowder of gamma phase aluminium oxide as binder. During mixing, for 15.00 g of zeolite and 6.43 g of binder, resulting in a mixture of 30 % binder and 70 % zeolite, 9.5, 8.5, and 10.8 mL of ultrapure water was added for MFI-25, MFI-38 and MOR-20, respectively.

After the pellets are formed, drying is necessary to achieve better mechanical properties of the material and remove water. Catalyst shaping is crucial, because the direct use of powder in a fixed-bed results in high pressure drop; furthermore, shaping improves heat distribution and chemical properties [43]. The samples were dried for 12h at 393 K and calcined at 823 K for 4 hours, then placed into a desiccator to cool down slowly and avoid adsorption of water.

BEA-35 was shaped by co-workers, without the addition of binder, into cylindrical pellets of 4 mm diameter and 2 mm height, using uniaxial compression in a benchtop model tablet press (TPD 1.5) with a maximum impulse force of 15 kN [19]. MFI-30 and MOR-40 were shaped by outside suppliers and it is not known the percentage of binder.

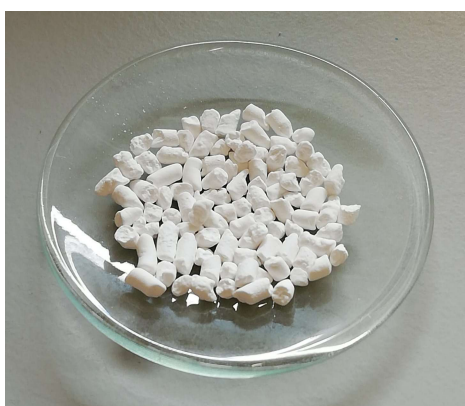
A photograph of each catalyst is presented in Figure 18.



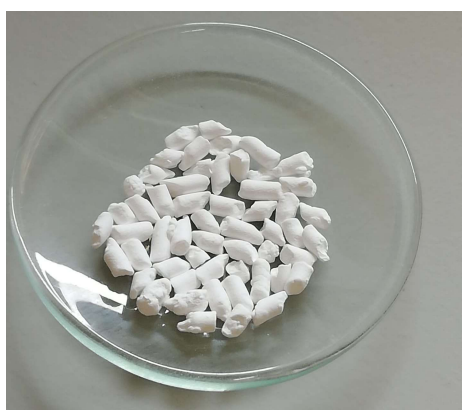
MFI-25



MFI-30



MFI-38



MOR-20



MOR-40



BEA-35

Figure 18. Digital photograph of all catalysts used: MFI-25, MFI-38 and MOR-20 were shaped at LSRE, while MFI-30 and MOR-40 were shaped by outside companies, and BEA-35 was shaped using uniaxial compression.

3.4 Catalyst Characterization

Catalyst characterization studies were made in order to understand the intrinsic features of each catalyst and comprehend the impact that morphology, textural characteristics, and chemical properties have in the reaction performance.

3.4.1 Textural Characterization

- **X-Ray Diffraction (XRD)**

Molecular structure of the crystal of every catalyst was studied by X-Ray Diffraction (XRD) to verify if the samples correspond to the respective structure. In order to do so, every result was compared to the reported powder pattern given by the International Zeolite Association (IZA).

XRD was performed in University of Málaga using Empyrean diffractometer from Panalytical at an accelerating voltage of 45 kV and an emission current of 40 mA with Cu $K\alpha_1$ ($\lambda=1.5405980 \text{ \AA}$) radiation. Measurements were performed for the angle (2θ) ranging from 5° to 80° for 30 minutes.

- **Crushing Strength**

The crushing strength tests were performed by Delft Solids Solutions, in Delft, the Netherlands, using Dr. Schleuniger type 5Y tablet harness tester, where approximately 50 particles were laid down automatically in the most stable position and then crushed by the side, in order to measure the radial crushing strength.

- **Scanning Electron Microscopy (SEM) and Energy Dispersive X-Ray (EDS)**

To study morphologic features and surface elemental composition, all catalysts were characterized by scanning electron microscopy (SEM) and energy dispersive X-ray (EDS), at Centro de Materiais da Universidade do Porto (CEMUP) using the equipment FEI Quanta 400FEG ESEM / EDAX Genesis X4M.

- **Nitrogen Adsorption at 77 K, Carbon Dioxide Adsorption at 273 K, and Mercury Intrusion**

Nitrogen adsorption at 77 K and carbon dioxide adsorption at 273 K were performed in Laboratorio de Sólidos Porosos, Servicios Centrales de Apoyo a la Investigación (SCAI) from University of Málaga, using a Micromeritics ASAP 2420 Accelerated Surface Area and Porosimetry System (USA). Mercury Intrusion was performed in the same facilities and the equipment used was a Micromeritics AutoPore IV 9500 Series (USA).

3.4.2 Acid Sites Characterization

Acid sites characterization is of the most importance. Differences in number, nature, and strength will influence overall reaction performance. Thus, to study the strength of the acid sites and its distribution, Temperature Programmed Desorption (TPD) was performed using ammonia (NH_3) as probe molecule.

TPD was performed at LSRE-LCM in an AMI-200 unit (Altamira Instruments), by placing 100 mg of zeolite in a U-shaped quartz tube. Thermal pre-treatment of the sample was performed at 873 K under helium atmosphere, afterwards the system was cooled down to 373 K and then adsorption for 2 hours of a helium stream with 5 wt% NH_3 . To remove physical adsorption, the system was flushed out with helium for 1 hour and finally heated up to 1173 K at a temperature rate of $10 \text{ K}\cdot\text{min}^{-1}$.

3.5 Experimental Setup and Procedure

The experimental setup is described in Figure 19. This experimental setup runs three different processes: catalyst drying, catalyst regeneration, and reaction.

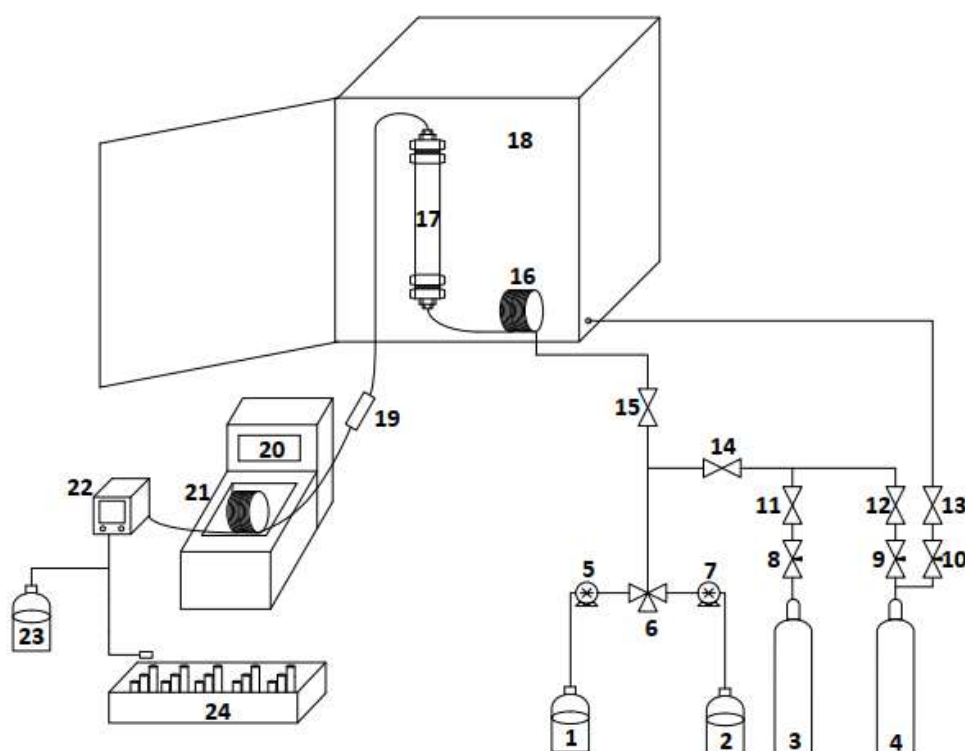


Figure 19. Experimental setup of the fixed-bed system: (1) Heptane bottle, (2) feed mixture, (3) air supply, (4) nitrogen supply, (5, 7) HPLC pumps, (6) three way valve, (11, 12, 13, 14, 15) on-off valves, (8,9, 10) needle valve, (16, 21) serpentine coil, (17) fixed-bed column, (18) oven, (19) in-line filter, (20) thermostatic bath, (22) back-pressure regulator, (23) waste bottle, (24) auto sampler.

The set of valves (6, 8, 9, 11, 12, 14, 15) can select what compound is the inlet of the column and control its flow rate; aromatics for reaction, n-heptane for purging, or gases for drying and regeneration of the catalyst. For safety measures, valves (10, 13) are intended to ensure an inert atmosphere inside the oven, in order to avoid explosive mixtures, while valves (9, 12) are set to catalyst drying and regeneration.

The feedstock goes into an oven (18), responsible to keep the reaction in controlled temperature conditions and the feed preheating to the desired temperature is done in the serpentine coil (16). For EB/Tol experiments, the feed mixture, bottle (2), was placed on a magnetic stirrer to ensure good agitation of the solution and avoid concentration differences through gravity sedimentation.

After going through the column (17), the outlet passes through a filter (19) to remove any particle or dust of the catalyst. To avoid evaporation, the stream passes through a serpentine (21) in a water bath (20) at room temperature. Finally, the flow is controlled by a back-pressure regulator (22) before being collected in the samples at atmospheric pressure.

The drying process was operated at 473 K for 12 hours with nitrogen flow, while catalyst regeneration consists in a temperature programme for three days with a mixture of nitrogen and air, resulting in a nitrogen flow containing 3% of oxygen. The regeneration temperature history is represented in Appendix A.

For the reaction experiments, the column is heated to the desired temperature, 513 K, with constant flow of n-heptane at 2.1 MPa. When the desired temperature is reached, the inlet is changed to the aromatic feed, always at 3 mL·min⁻¹ and 2.1 MPa. The volume obtained during a given period of time was measured several times, in order to confirm the flow rate provided by the HPLC pump (7).

When the reaction experiment is completed, the oven is turned off and the inlet is changed back to heptane to cool down and to purge the column. Reaction is always followed by drying and catalyst regeneration. To ensure catalyst regeneration was effective, at least one experiment was repeated after regeneration for each catalyst, to ensure that there was no loss of activity.

Every sample collected was analyzed by gas chromatography (GC) in GC-2010 Plus from Shimadzu equipped with a flame ionization detector (FID) and a SGE-BP20 (Wax) column with polyethylene glycol, which is a very polar phase suited for analysis of aromatic compounds with good separation of isomers like xylenes. This column has a length of 25 m, an inner diameter of 0.53 mm and a film thickness of 1 µm.

Two different GC methods were used depending on outlet composition. If only isomerization and disproportionation of xylene occur, a faster method was used, where TMBs are the last

compounds to be analyzed. Meanwhile, in case of PDEB isomerization, triethylbenzene can be formed by diethylbenzene disproportionation. In this case, the method was changed by adding a second temperature ramp, which increases the analysis time. Two examples of chromatographs are represented in Appendix B, one for each method. As seen, it was tried to resolve every peak, even though separation of PX and MX, as well as *m*-diethylbenzene (MDEB) and *p*-diethylbenzene (PDEB) is very difficult. The rule of thumb which states that peaks should only be observed in an temperature plateau region was followed.

The catalysts were packed in columns made of 316 stainless steel, with glass wool in both ends. Every column was subject to the following procedure:

1. Weighing of empty column with closed caps
2. Weighing of column with the first piece of glass wool
3. Measurement of initial length of the column
4. Weighing of column with one piece of glass wool and catalyst
5. Measurement of final catalyst length
6. Weighing of the final column with a second wool at the end
7. Weighing of the column after overnight drying at 473 K and under constant flow of nitrogen

4 Results and Discussion

4.1 Textural Characterization

- XRD

XRD results are represented in Figure 20.

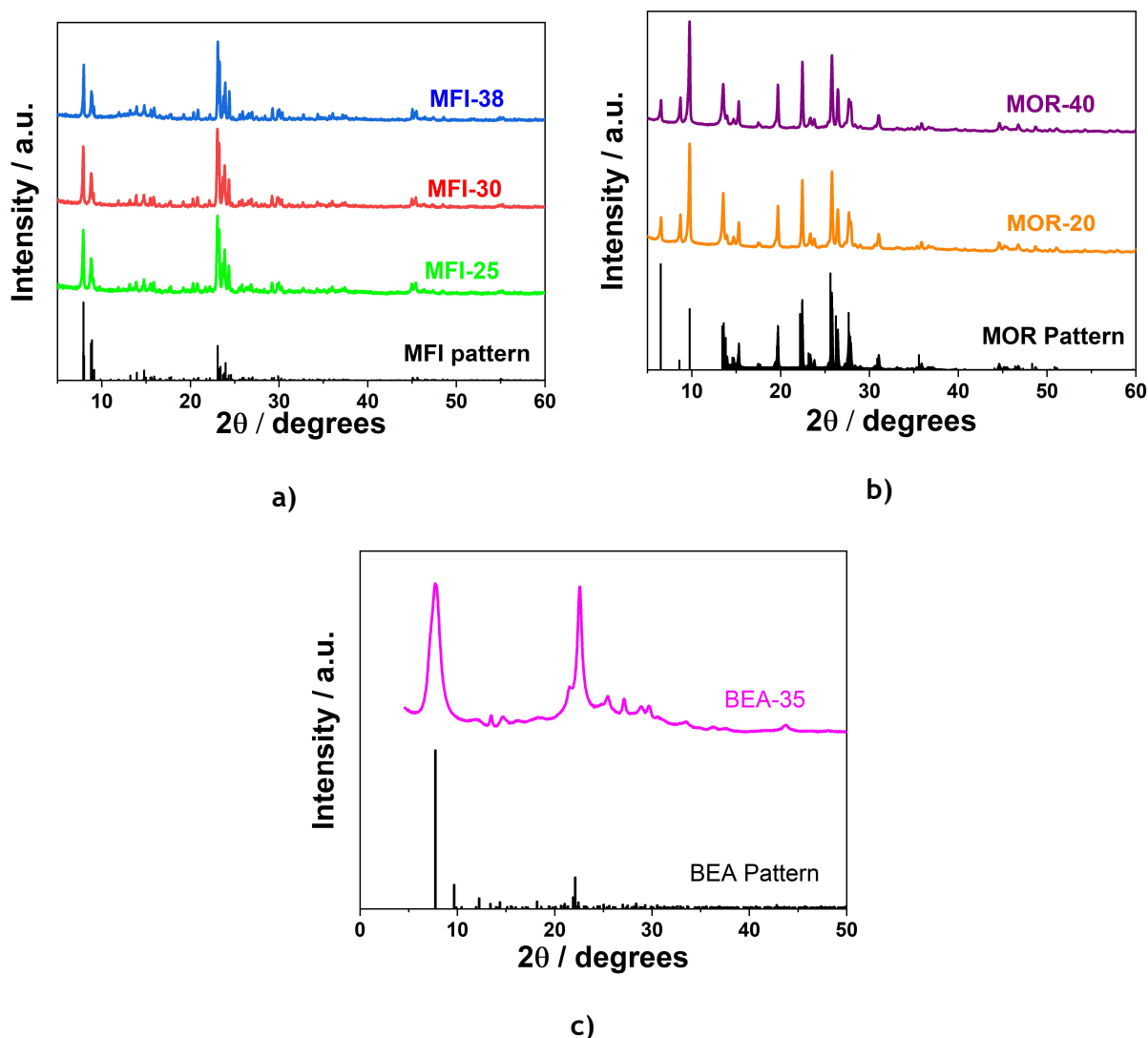


Figure 20. XRD comparison of the a) MFI, b) MOR, and c) BEA samples against the respective IZA's pattern.

As seen in Figure 20a, after shaping, all MFI samples retained the classic XRD features of MFI topology, namely the double peak at 7° - 9° and triple peak at 23° - 25° , resulting in a very pure crystal structure. MOR (Figure 20b) and BEA (Figure 20c) catalysts showed the same results, by overlapping of the same peaks between IZA's pattern and samples. Hence, the manufacture by external companies or using in-lab equipment, even the extrusion and the thermal treatment

did not compromise the actual structure, as well as the fact that the products formed are free from impurities and are highly crystalline.

Crushing Strength

Crushing Strength results are presented in Table 4.

Table 4. Crushing strength results

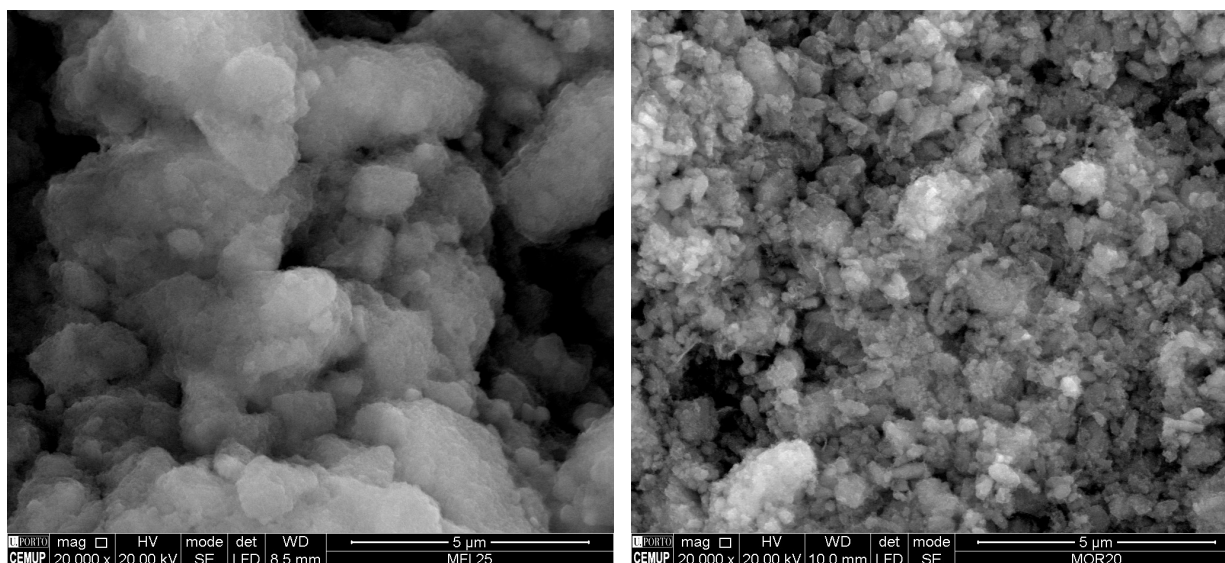
		MFI-25	MFI-30	MFI-38	MOR-20	MOR-40	BEA-35
Number of Particles	-	50	50	50	50	50	50
Average	N	8.2	25.4	13.1	6.8	33.2	54.8
Standard deviation	N	3.2	14.5	5.1	6.5	11.4	28.8
Relative standard deviation	%	39.0	57.0	39.0	96.0	34.0	53.0
95 % confidence interval	N	0.9	4.1	1.4	1.8	3.2	8
Minimum	N	4	3	6	1	3	5
maximum	N	21	49	29	19	74	114

MFI-30, BEA-35 and MOR-40 have higher crushing strength, which can be explained by their typical cylindrical (MFI-30 and MOR-40) or slab form (BEA-35), while other catalysts have rounded surfaces.

MFI-30 shows the particularity of having 2 different ranges for strength: a minority of extrudates below 7 N and the majority above 22 N; similarly, MOR-40 showed the same behavior, 26 particles below the lower measuring limit, being weaker than 2 N, therefore MOR-40 crushing strength is overestimated since for these pellets in particular it was assumed 1 N for calculations.

- **SEM**

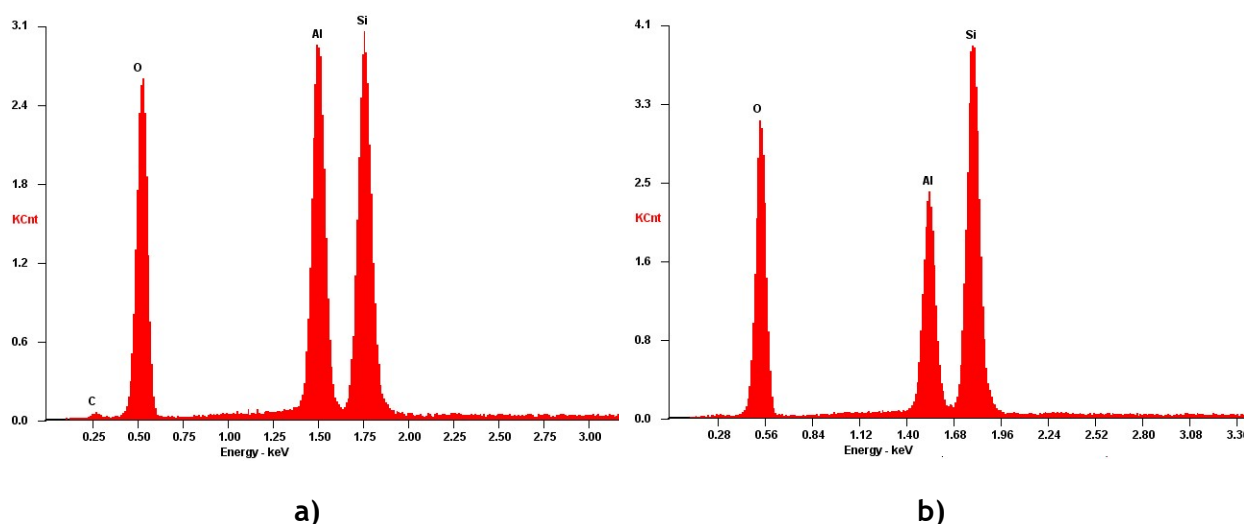
All SEM and EDS results are presented in Appendix C, although for MFI-25 and MOR-20 the results are shown in Figure 21 and Figure 22. Only the typical elements for zeolites of this type were found in the EDS results.



a)

b)

Figure 21. SEM images for an amplification of 20000x of MFI-25, a), and MOR-20, b).



a)

b)

Figure 22. EDS results for MFI-25, a), and MOR-20, b).

Through comparison of all the SEM images presented in Appendix C, it is easy to conclude that there are some differences between the zeolites. MFI-30 has separated crystals, while for MFI-25 and MFI-38 it is hard to visualize the primary particles due to agglomeration. MOR samples have smaller crystal size than MFI catalysts. Additionally, there were no significant differences between MOR-20 and MOR-40. BEA-35 crystals are very easy to identify and seems that agglomeration is less pronounced than any other catalyst.

- **Mercury Porosimetry and Adsorption of N₂ and CO₂**

Mercury porosimetry was performed to evaluate the macropore size distribution. In Figure 23, it is compared all MFI-type catalysts, while in Figure 24 MOR-type catalysts and BEA are compared.

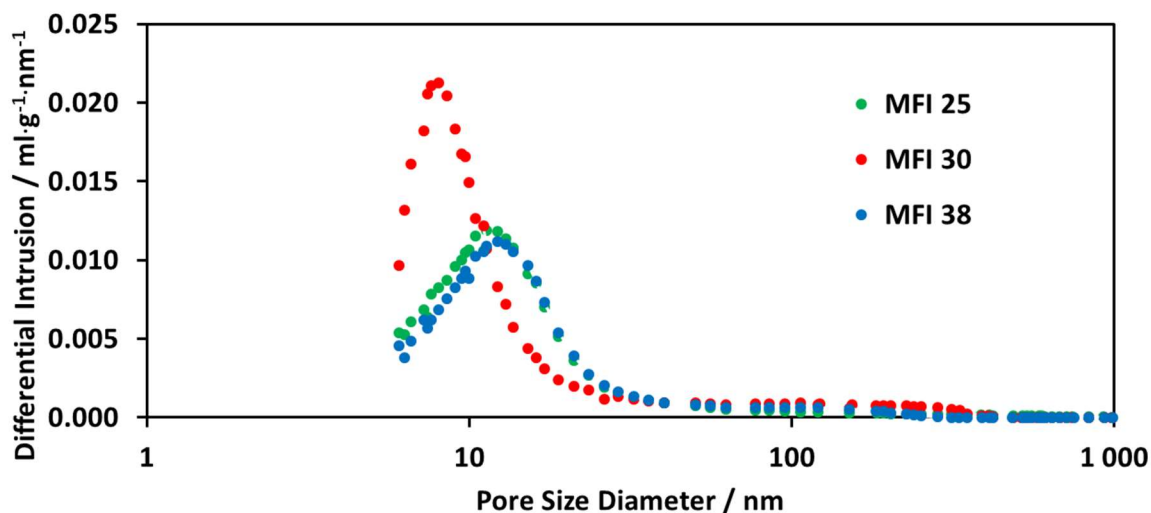


Figure 23. Pore size distribution by mercury porosimetry for MFI-type catalysts.

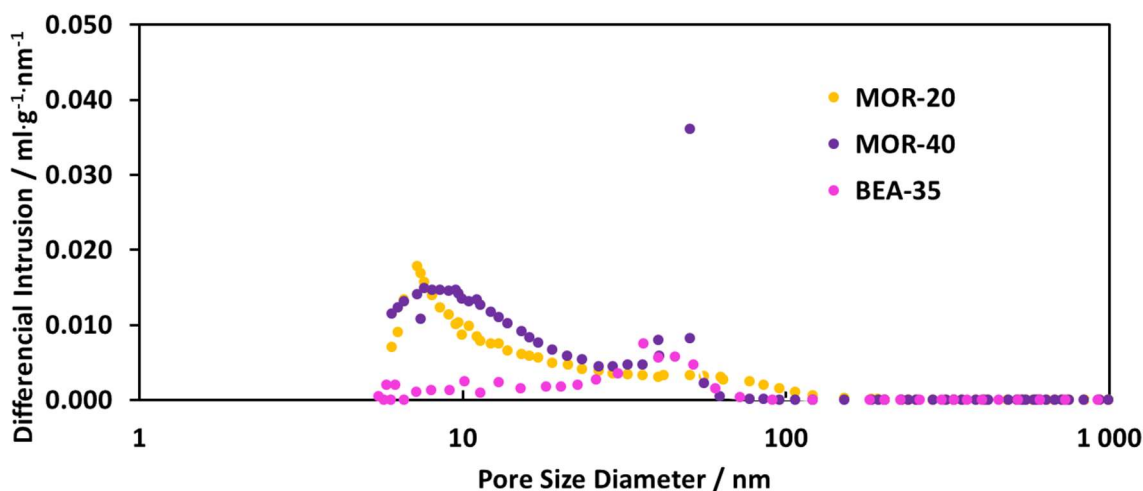


Figure 24. Pore size distribution by Mercury porosimetry for MOR-type catalysts and BEA-35.

From Figure 23, one can conclude that MFI-25 and MFI-38 have very similar pore distribution with same average diameter, around 13 nm, while MFI-30 offers a narrower pore distribution with smaller mesopores, with an average diameter of 8 nm. Differences can be explained by the fact that MFI-30 was produced and shaped by an external company, while MFI-25 and MFI-38 pellets were produced in the same equipment and using the same protocol. Thus, the macropore/mesopore size seems not to be dependent of the Si/Al ratio, but by the equipment and shaping procedure.

Conversely, from examination of Figure 24, all mordenite samples showed higher quantity of intruded mercury in the mesopores range (2-50 nm) than BEA-35, also evidenced by the nitrogen isotherms of Figure 26. However, BEA-35 shows a wide range of mercury intrusion in the region of larger mesopores to macropores. Additionally, MOR-40 shows a bimodal

distribution of pores, one peak at the small mesopores interval and another peak evidenced the region around 50 nm of pore size diameter.

Adsorption equilibrium isotherms of nitrogen at 77 K are represented in the Figure 25 and Figure 26 and carbon dioxide isotherms at 273 K are represented in Figure 24 and Figure 25.

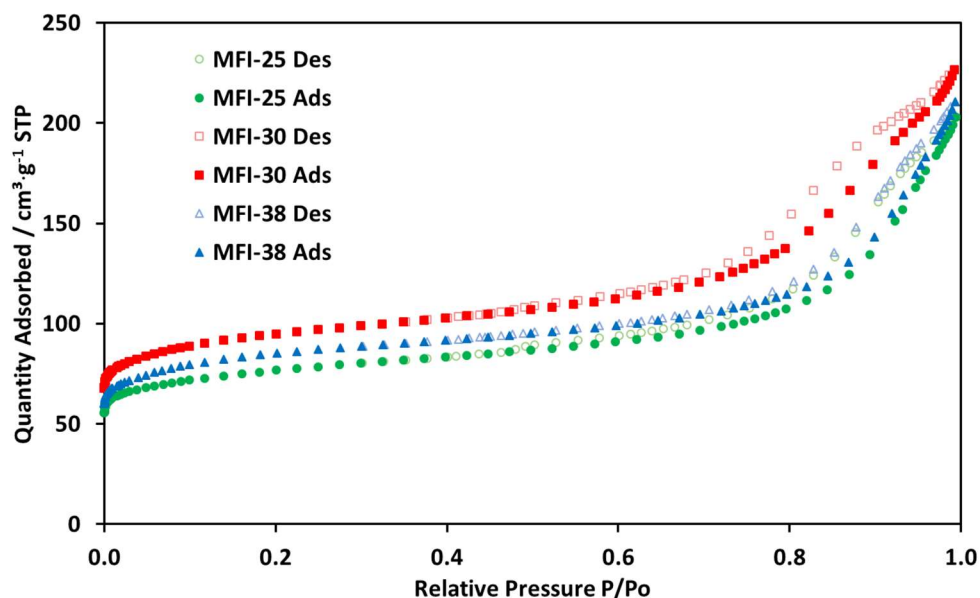


Figure 25 Nitrogen adsorption isotherm at 77 K for medium-pore catalysts.

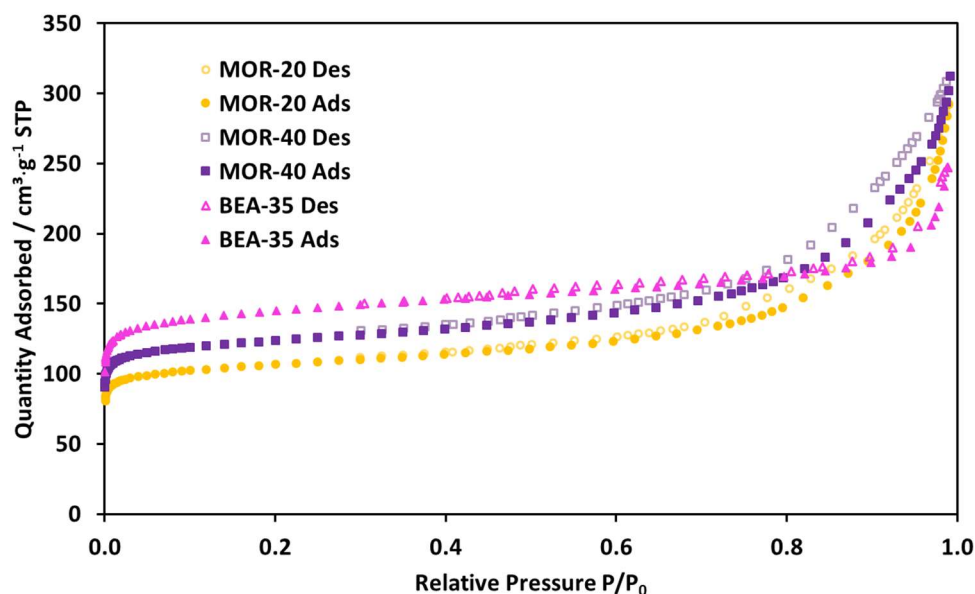


Figure 26. Nitrogen adsorption isotherm at 77 K for large-pore catalysts.

From Figure 25 and Figure 26 is possible to observe the presence of microporous by rapid adsorption at mainly narrow pores, reassembling the type I(a) isotherm for very low pressures. For high relative pressure, $P/P_0 > 0.8$, the increase is justified by adsorption on the mesopores.

The obtained isotherms are characteristic of shaped zeolites, which are known by their microporous structure, and secondary meso/macropores network derived from the shaping.

From Figure 25 it is easily verified that MFI-30 has higher surface area. This should give advantage in terms of reaction performance. Similarly, MOR-40 has higher surface area than MOR-20. It is important to notice the differences between BEA and MOR catalysts, the former shows higher adsorption in the lower region of relative pressures, but only shows considerable increase after pressures around 0.9, while the latter show abrupt increase in adsorption after relative pressure 0.8, therefore MOR samples should have higher quantity of mesopores. This mesoporous network can give advantage in terms of reaction, due to the facilitated transport inside these pores, while the higher volume of microporous of BEA-35 can possibly hinder the transport of the molecules.

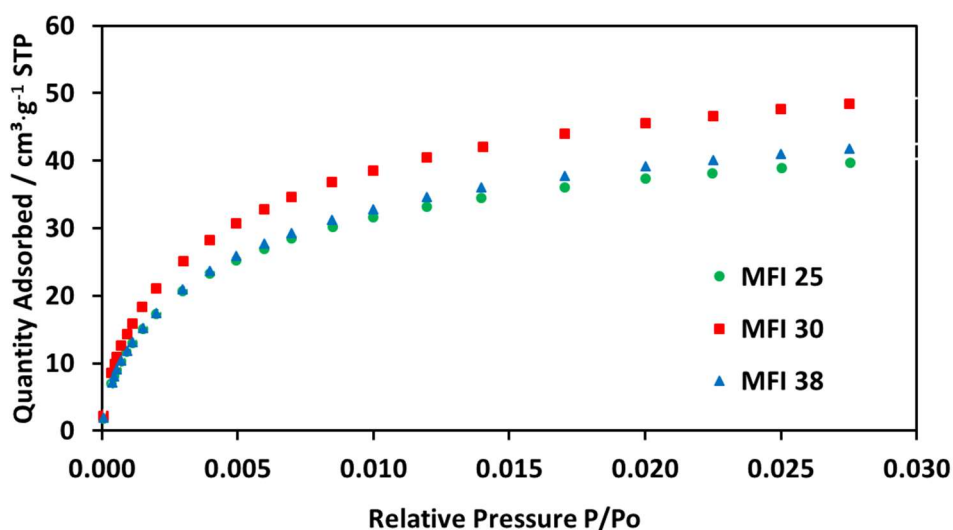


Figure 27. Carbon Dioxide adsorption isotherm at 273 K for medium-pore catalysts.

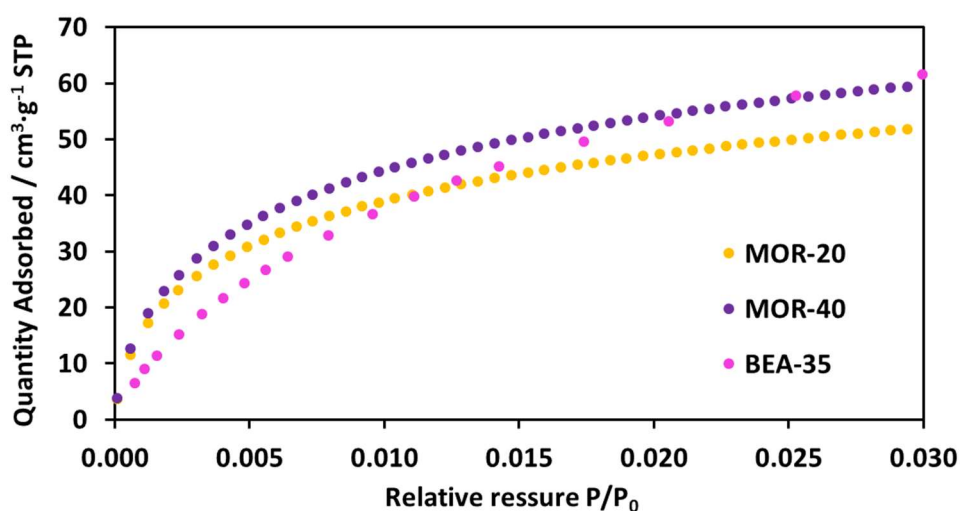


Figure 28. Carbon Dioxide adsorption isotherm at 273 K for large-pore catalyst.

Table 5. Results from Mercury intrusion and adsorption of N₂ and CO₂.

	Apparent Density ^a	Particle Porosity ^a	Langmuir Surface Area ^b	Micropore Volume ^b
	g·mL ⁻¹	%	m ² ·g ⁻¹	cm ³ ·g ⁻¹
MFI-25	1.11	45.7	352 ± 2	0.0894 ± 0.0001
MFI-30	1.06	47.6	436 ± 2	0.1081 ± 0.0004
MFI-38	1.21	40.2	393 ± 2	0.1037 ± 0.0002
MOR-20	1.03	48.6	480 ± 2	0.1267 ± 0.0004
MOR-40	0.95	41.9	557 ± 3	0.1455 ± 0.0005
BEA-35	1.05	28.7	653 ± 2	0.198 ± 0.001

a: Results obtained by mercury intrusion; b: Results obtained by nitrogen adsorption at 77K

CO₂ adsorption at 273 K, Figures 25 and 26, was performed to understand if the higher diffusion due to higher temperatures would cause an appreciable increase of adsorption in the micropores, which was not observed, therefore micropore volume was calculated using nitrogen adsorption at 77 K.

In Table 5, the most important parameters obtained by mercury intrusion and nitrogen adsorption are presented for every catalyst. From the MFI-type catalysts, MFI-30 shows the highest surface area, which should give better reaction performance. Large-pore catalysts showed higher surface area than medium-pore catalysts, particularly BEA-35.

4.2 Acid Sites Characterization

Desorption is an endothermic reaction, therefore when there is an increase on the temperature, molecules will desorb in function of how strongly the bond between the molecule and the acid site is. This strength is related with acid site strength: strong acids will bond strongly and NH₃ will desorb at higher temperatures, while NH₃ in weak acids will desorb at lower temperatures.

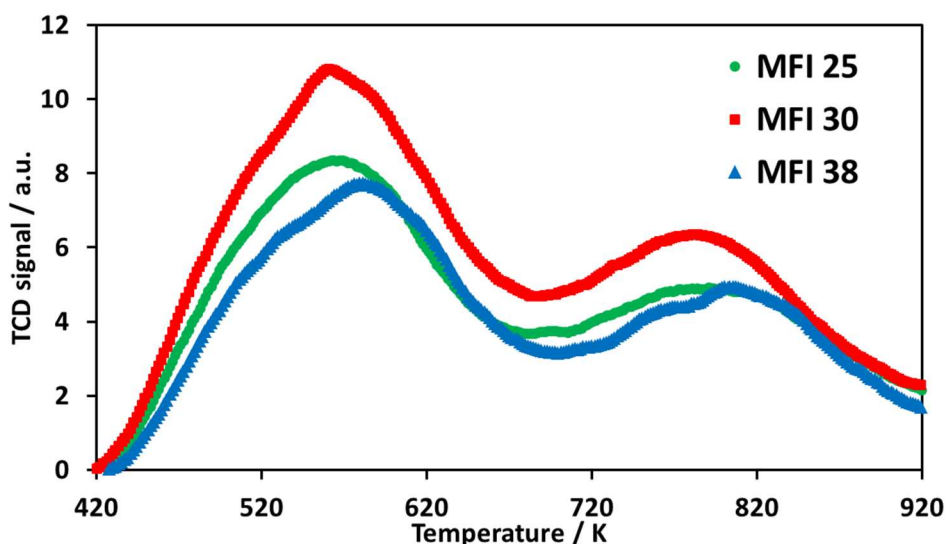


Figure 29. TPD results of ammonia from MFI series.

From Figure 29 it is possible to conclude that the MFI-type catalysts have essentially weak and strong acid sites. Weak acid sites are in bigger quantity for every catalyst, especially MFI-30 which has the highest number of overall sites. MFI-38 shows a little deviation towards higher temperatures, but is the one with least amount of acids, hence confirming that as the $\text{SiO}_2/\text{Al}_2\text{O}_3$ ratio increases its strength increases due to separation between Al atoms [30]. The differences between various zeolites should be pondered according to the synthesis procedure and not exclusively to the influence of $\text{SiO}_2/\text{Al}_2\text{O}_3$ ratio [44]. The unknown binder amount used in MFI-30 synthesis could explain this difference.

4.3 Column Characterization

In Table 6, the most important parameters of each packed column are summarized.

Table 6. Column characterization.

	MFI 25	MFI 30	MFI 38	MOR 20	MOR 40	BEA 35
Column diameter D (cm)	2.1	2.1	2.1	2.1	2.1	2.1
Column height L (cm)	28.8	29	29.1	29.3	28.3	31.1
Dry catalyst mass W_c (g)	70.3	60.4	78.7	60.0	66.2	70.6
Water released after drying (g)	4.2	6.3	2.7	0.9	8.0	9.3
Bed porosity ϵ	0.36	0.43	0.35	0.42	0.30	0.38

Calculation of the quantity of water released after drying is by no means a pragmatic test to evaluate the hydrophilic character or the amount of acid sites, but could be used to estimate a trend, because it has been pointed that water adsorption is a function of $\text{SiO}_2/\text{AlO}_3$ ratio, as well as pore structure and size [45]. For the MFI-type catalysts, the amount of water adsorbed

showed correlation with acidity, thus the higher acidic catalyst, MFI-30, had higher quantity of water. MOR-20 released a low quantity of water, most likely because it was packed shortly after being shaped and dried, while the others were stored for a longer time. However, drawing conclusions from the $\text{SiO}_2/\text{Al}_2\text{O}_3$ ratio without taking into consideration the acid characterization could be misinterpreted, especially if zeolites were synthesized by different methods.

4.4 Reaction Results

4.4.1 Xylene Isomerization

The steady state reaction results obtained for each catalyst are presented in Table 7 and were obtained using Equations (1) and (2). Additionally, it was calculated the external and internal mass-transfer resistances, the procedure and equations are found in Appendix D. No mass-transfer limitations were found in the experiments.

Table 7. Reaction performance parameters for each catalyst

	MOR-20	MOR-40	BEA-35	MFI-25	MFI-30	MFI-38
$R_{\text{obs}} \times 10^7 / \text{mol} \cdot \text{g}_{\text{cat}}^{-1} \cdot \text{s}^{-1}$	23.3	28.1	17.9	2.6	2.8	1.1
Conversion %	34.4	45.3	30.9	4.4	4.1	2.0
Secondary Products %	0.3	1.9	3.1	0.0	0.0	0.0
Selectivity PX	1.1	1.1	1.3	3.6	3.9	3.3

$$R_{\text{obs}} = \frac{(C_{\text{in}} - C_{\text{out}})Q}{W} \quad (1)$$

where the observed reaction rate for a heterogeneous system, R_{obs} , was calculated by using Equation 1, where C_{in} and C_{out} are respectively the concentrations of reactant at the feed and outlet of the fixed-bed, while Q denotes for flow rate and W_c for catalyst dry mass.

Similarly, reactant conversion was calculated by Equation 2, which is valid for constant volume.

$$X = \frac{C_{\text{in}} - C_{\text{out}}}{C_{\text{in}}} \quad (2)$$

Secondary products percentage was calculated by simple sum of the secondary products mole percentage, while selectivity was calculated by the quotient between PX and OX product concentration.

Undoubtedly, large- and medium-pore catalysts differ significantly from each other. For approximately the same column length, large-pore catalysts have almost ten times more conversion; although having a higher, yet small, percentage of secondary products, between 2

to 3 %. On the other hand, the reduced size of medium-pore zeolites offers high selectivity towards PX, while large-pore catalysts have no selectivity at all.

To a better differentiation between all MFI-type catalysts, it is represented its concentration profiles in Figure 30.

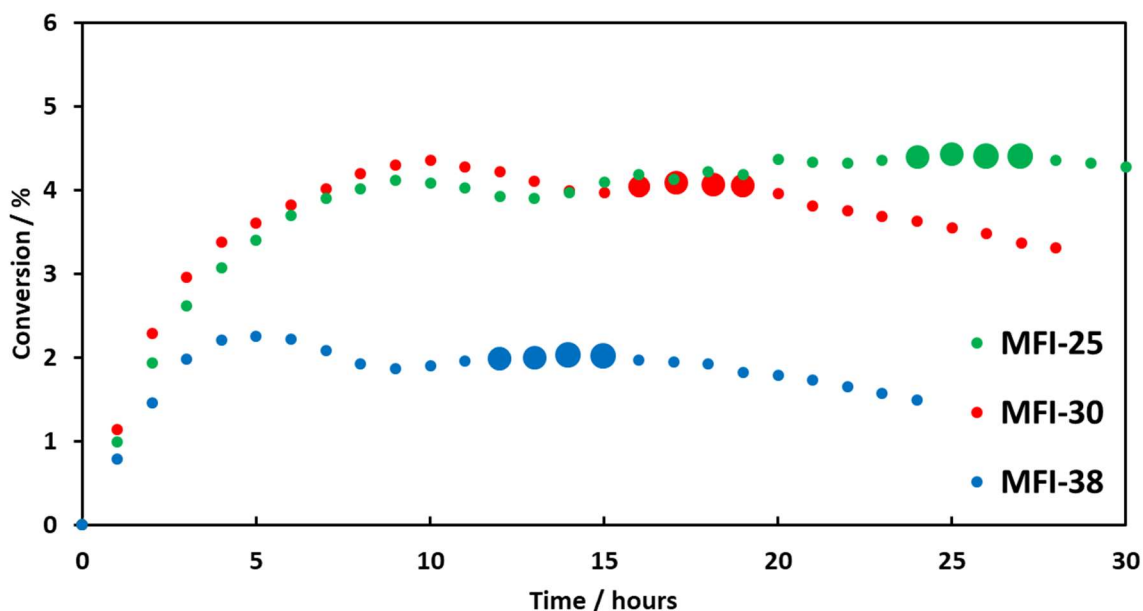


Figure 30. Concentration profiles for each MFI-type Catalysts. Steady state points were intentionally augmented to facilitate observation.

MFI-38 obtained the worst results between the three, which is somewhat expected due to the lower amount of acids. Surprisingly, MFI-25 has a little more quantity of acids than MFI-38, but still fewer than MFI-30, nevertheless had the highest conversion, as seen from Table 7.

At first glance, one could say that MFI-25 is a better alternative to MFI-30, but these results should be confronted with the column characterization, because for a higher mass of catalysts the conversion may be higher. For the same column length, MFI-25 has higher mass of catalyst, this is explained by better packaging of the catalyst inside the column, due to its intrinsic rounded geometrical features created in the spheronization process during catalyst shaping; conversely, the cylinder shaped of MFI-30 hampers the packaging. These geometrical features are differentiated in Figure 18. Thus, to compare MFI-25 and MFI-30, one should use the observed reaction rate, which is normalized by the quantity of dry catalyst, this way MFI-30 is the best MFI catalyst in reactant transformation. This statement goes accordingly with the catalyst characterization, MFI-30 excel the others catalysts in acids sites amount and surface area, as seen from Figure 29 and Table 5.

Considering the acid characterization in Figure 29, the differences on conversion between MFI-25 and MFI-38 were more pronounced than foreseen, this could be attributed to the

synthesis of the zeolite powder. Even if indeed they have somewhat the same amount of total acids, more pronounced difference could exist between the nature of the sites, meaning that MFI-25 could have a higher quantity of Brønsted acids, which contribute to the catalysis of this reaction. Unfortunately, no Fourier Transform Infrared Spectroscopy (FTIR) was performed yet.

The curves for the concentration profile seem to have a first maximum followed by some decline and a relative maximum before deactivation. This behavior could be explained by evolution of different secondary reactions or by an activation period that some catalysts often suffer.

The PX selectivity and the percentage of secondary products show how the MFI-type has two different types of selectivity. One is the shape selectivity of the narrow structure of this zeolite, which facilitate the diffusion of PX over OX and MX that have higher diffusion constraints. On the other hand, this catalyst also shows restricted transition-state selectivity; the transition-state of xylene disproportionation reaction, tri and tetra methylated diphenylmethane, does not have enough space to be formed, therefore only isomerization reaction occurs [21, 46]. However, it should not be forgotten that the secondary reactions, as well as deactivation are function of conversion. In order to have a better understanding, experiments with higher conversion should be conducted.

From Figure 31, two things stand out: the high conversion and the rapid deactivation shown by large-pore catalysts. For these catalysts, the parameters of Table 7 were calculated considering the maximum concentration in each run; although for BEA-35 the maximum is most likely a compromise between simultaneous reaction and deactivation processes, opposed to MOR-40, which shows longer lasting steady state.

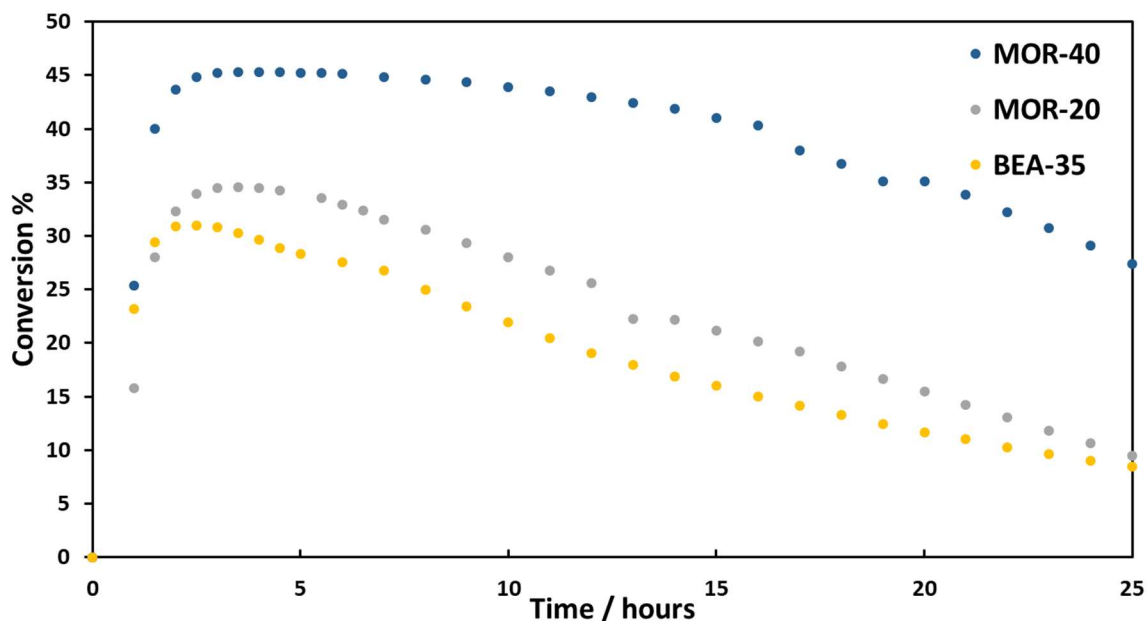


Figure 31. Large-pore catalysts conversion as function of time of each experiment.

By having higher channel diameter, these catalysts allow a better diffusion of all molecules, hence the reactant has easier access to the acid sites, but this comes with the disadvantage of high diffusion of other products such as OX, therefore no selectivity between PX and OX was found.

Among the large-pore catalysts, MOR-40 showed the best performance, while BEA-35 was the worst catalyst. It seems that the bigger channels and the higher quantity of mesopores, evidenced in Figure 26, offers better conditions to MOR. Additionally and without further information on acid sites, the outperformance of MOR-40 could be explained by the existence of a bimodal pore network, evidenced in Figure 24, which may have increased the mass transport of the aromatic species leading to higher conversion.

In contrast of medium-pore catalysts, now the bulky intermediate, tri and tetra methylated diphenylmethane needed to form TMBs, has enough space to be formed; therefore, there is some disproportionation of xylenes and the xylene isomerization reaction is in grand part attributed to bimolecular mechanism, which has

Deactivation by coke is faster if there is a larger space near the acid site, so theoretically large pore-type catalysts should expect higher deactivation. But the intrinsic catalyst structure, the acid sites density and strength distribution also affect deactivation. Thus, MFI-catalysts showed mild deactivation, but more experiments should be done in order to fully understand how these catalysts deactivates in a conversion range similar to those of the large-pore catalysts, because if the reaction rate is low, then the deactivation will be low too. MFI-type catalysts deactivation can be explained by the lack of available space inside the crystal to form heavy weight coke

precursors and the fact that they typically have low density of acid sites, indeed these reactions need two active sites near to each other, and this will be more difficult [47].

Meanwhile, the rapid deactivation of mordenite can be explained by its unidimensional pore structure, so once a channel is deactivated by pore blockage every acid site in it will be unutilized. This justification is often used to explain MOR deactivation, but at the same time seems inadequate, because molecules can access the pore by the other end and exit by the same entrance by counter-diffusion, either way the transport is considerably more difficult, allowing the coke precursors to grow.

MOR-20 had a faster deactivation than MOR-40, this could be explained by the difference on acid sites density; indeed, MOR-40, by having higher quantity of $\text{SiO}_2/\text{Al}_2\text{O}_3$, should have the acid sites more distant from each other, resulting in a lower formation of heavy aromatics.

Finally, BEA showed even faster deactivation; this could be explained by the bigger space due to a 3D interconnected channel structure that allows formation of coke molecules. Additionally, due to smaller pore dimensions, coke molecules could have slower diffusion in comparison with mordenite and by this way staying longer in the catalysts without being flushed out of the reactor by the liquid phase [47]. In fact, as seen in Table 7, BEA-35 had the most quantity of secondary products, while MOR-40 has the least, which goes accordingly with the deactivation profiles stated in Figure 31.

With these results, the most viable catalyst to integrate an SMBR unit is the MOR-40, because it can convert more reactants, which is the main requirement of this type of unit, has the least quantity of secondary products and has the slower deactivation among the large-pore catalysts.

4.4.2 Ethylbenzene and toluene

Experiments using 50 % wt mixture of ethylbenzene and toluene were performed. Ethylbenzene conversion for MFI-25 was around 1.0 % and for MOR-20 2.0 %; while toluene conversion was 0.4 % for MFI-25 and 0.7 % for MOR-20. Experimental conversion in function of time can be found in Appendix E.

Ethylbenzene can react with itself by two different reactions: disproportionation, which involves the formation of bulky intermediates, such as diphenylethane, or by dealkylation followed by alkylation of other ethylbenzene molecule. The latter has a lower reaction rate and for medium-pore catalyst this mechanism is favored, due to space limitations to form bulky intermediates, while for large-pore catalyst most of ethylbenzene transformation is due to disproportionation [48]. This explains why MOR-20 had higher conversion than MFI-25.

Both catalysts convert EB and the small difference between them do not invalidate the viability of mordenite to be used as a catalyst in an SMBR; in fact, even if ethylbenzene conversion was

the double than on MFI-25, xylene conversion was around 10 times more for MOR-20. EB disproportionation and EB and Tol disproportionation do not seem to occur extensively in both catalysts, therefore toluene can be good candidate to be used as a desorbent in a SMBR.

4.4.3 *P*-diethylbenzene (PDEB) Isomerization

In order to evaluate if PDEB could be used in an SMBR as a desorbent, similar experiments to the previous ones were performed using MFI-25 and MOR-20. The results are described in Table 8 and conversion profiles at Figure 32.

Table 8. PDEB isomerization results

	MFI-25	MOR-20
$R_{obs} \times 10^6 / \text{mol} \cdot \text{g}_{cat}^{-1} \cdot \text{s}^{-1}$	1.5	3.9
Conversion %	31.9	72.6
Secondary Products %	0.2	10.0
MDEB/ODEB	125.6	10.7

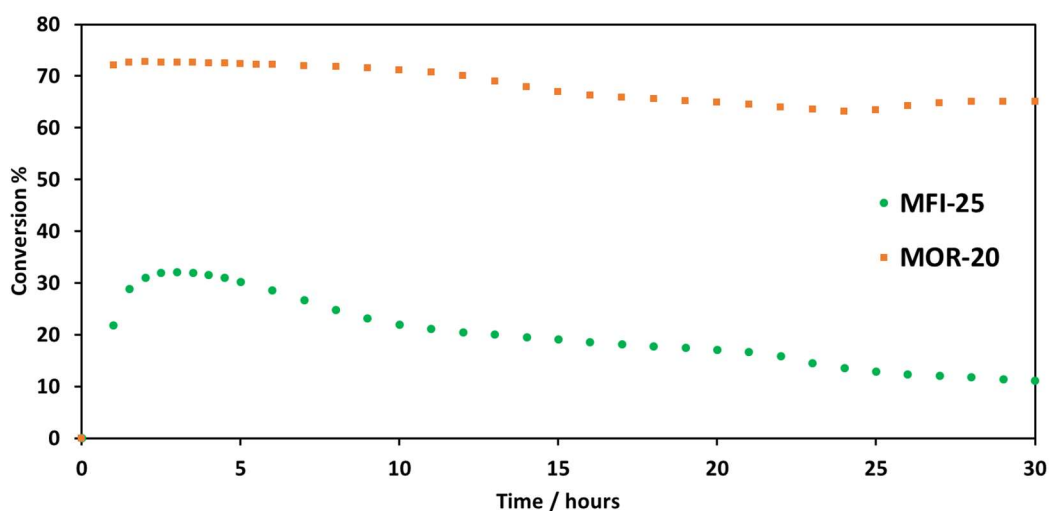


Figure 32. Conversion profiles for PDEB isomerization.

MFI-25 produced almost only *m*-diethylbenzene (MDEB), while *o*-diethylbenzene (ODEB) was not present in the product composition, most likely due to its bigger kinetic diameter and the reduced diameter of MFI catalysts in comparison with MOR. In fact, PDEB, MDEB and ODEB have respectively 6.63, 7.26 and 7.96 nm of minimum cross diameter [15]. It seems that ODEB does not have enough space in MFI-type catalysts to be formed. Also, it was not found 1,3,5-triethylbenzene; hence, for the same reason it seems that there is only space to form 1,2,4-triethylbenzene.

MOR-20 exhibited high proportion of MDEB with a small quantity of ODEB, it should be kept in mind that MDEB is favored by equilibrium. Bolton *et al.* studied the isomerization of diethylbenzenes using Y zeolite and for a 100 hr reaction time and 443 K, the relative

percentage of diethylbenzene products were 5% ODEB, 62% MDEB and 33% PDEB [49]. These percentages are very close to the ones obtained by MOR-20, therefore there is high probability that this experiment was limited by chemical equilibrium.

Similar to EB reactions, PDEB isomerization reaction can have both monomolecular and bimolecular mechanism. In MOR-20, PDEB may have undergone through bimolecular rearrangements, forming bulky intermediates; while in MFI-25, because of space limitation, this should not account for the total conversion of PDEB [49]. The higher conversion of PDEB in MOR-20 could be explained by a higher contribution of the bimolecular mechanism. It is concluded that PDEB cannot be used as desorbent, because it has a significant conversion for both catalysts.

5 Conclusions

The purpose of this work was the study of xylene isomerization reaction over acid catalysts in the liquid phase. The zeolites studied were MFI (medium-pore catalysts), BEA, and MOR (both large-pore catalysts). This work was highly motivated by the increasing interest on performing this reaction in the liquid phase and by the possible application of an SMBR unit to improve the reaction performance and energy consumption.

MFI has the smallest pore size and showed reduced conversions, but very good selectivity towards PX, the product with higher industrial interest. Meanwhile, BEA and MOR showed higher conversions, but do not have selectivity and showed some percentage of secondary products like Tol and TMBs.

MOR samples have better results of conversion in comparison with BEA catalyst, most likely due to the higher mesoporosity evidenced in the nitrogen isotherms at 77 K, but further evaluation of the acid sites by TPD-NH₃ or by FTIR should be made.

MOR-40 showed the best results. For 66.2 grams of dry mass, this catalyst obtained a conversion of 45.3 %, an observed reaction rate of $28.10 \times 10^7 / \text{mol} \cdot \text{g}_{\text{cat}}^{-1} \cdot \text{s}^{-1}$, 1.9% of secondary products, but did not show selectivity towards PX, yet was the catalyst with slower deactivation. These results could be explained by the existence of bimodal network and lower density of acids.

Thus, to be incorporated into an SMBR, MOR-40 was pointed as the best solution, because in this type of equipment the selectivity is provided by the adsorbent, therefore the conversion is the main requirement.

PDEB was excluded from being used in a SMBR as desorbent, due to very high conversions, while toluene showed to be a suitable candidate.

6 Assessment of the work done

6.1 Objectives Achieved

One of the objectives was to study the performance of various catalysts with different pore structure and acidity in the xylene isomerization reaction. This objective was fully achieved, where it was explained every reaction result by trying to conjugate the textural and chemical characterization and the fixed-bed reactions results, achieving this way a brief balance between how the catalysts characteristics influence the reaction conversion, selectivity, and secondary products.

Another objective was to select the best suitable catalyst for integration processes of separation and reaction in an SMBR unit; MOR-type catalysts seem to excel in this area, based on the high conversions, which is the most important requirement for an SMBR application.

6.2 Limitations and Future Work

These type of catalyst studies have several problems and/or limitations. Buying the same catalyst with the same $\text{SiO}_2/\text{Al}_2\text{O}_3$ ratio from different suppliers may result in very different products, due to different equipment, operators and synthesis procedures. The aforementioned will difficult the analysis and conclusions based on some parameters, for example, the $\text{SiO}_2/\text{Al}_2\text{O}_3$ ratio.

Meanwhile, fresh catalyst operates better than a regenerated sample, therefore the first experiment was always discarded, even if it takes time and consumables to execute it. In the experimental setup, the oven can only go to a maximum temperature of 400 °C, which seems unsuitable for a total regeneration. After regeneration, the experiments were repeated in order to see how different the activity of the catalyst was before and after being regenerated.

Indeed, the first plan for this thesis was the calculation of the kinetics of the best MFI-type catalyst, but the activity besides being low, it seemed significantly affected by regeneration. Thus, the regeneration procedure was extended to three days, instead of the original two days.

Additionally, in some experiments, as seen in Figure 30 and Figure 31, conversion can go through two maximums before deactivation. As previously said, this seems to be the interaction of equilibrium of multiple secondary reactions and by the deactivation process. This made it harder to analyze the results and led to increase the reaction time to 30 h, in order to see if there were multiple maximums and to be sure a declination of activity was due to deactivation. Obviously, taking many samples of a system with slow dynamics in a short period of time will

appear as some kind of steady state, longer experimental protocols should be executed in order to see if our judgment is not being misguided by this data virtualization.

The increase in regeneration and reaction time made the primary objective of reaction kinetics impracticable taking in account the time to finish this thesis, therefore improvements in such way to reduce the time should be investigated.

Deactivation studies should be interesting, particularly because they are scarce for catalyst deactivation of xylene isomerization reaction in the liquid phase. Aguayo et al. studied regeneration of HZSM-5 in the transformation of ethanol into hydrocarbons and it was achieved full regeneration for only 2h on stream for a regeneration temperature of 550 °C with air only as inlet [50]. Guisnet also studied extensively how pore size, pore structure, existence of cavities, and the dimensionality of the pores could affect both coke deactivation and composition [47].

Therefore, it is proposed as future work to study the effect on deactivation of pore structure of medium and large pore catalysts, with full evaluation of coke composition and acid site characterization after regeneration, because it is known that the presence of water can shift Brønsted acids into Lewis and any combustion reaction results in water, so an optimization of the regeneration process must be done.

Reaction kinetics of heterogeneous systems for xylene isomerization reaction in the liquid phase is also scarce, and it is an inevitable data that must be obtained in order to study the viability of the SMBR process. To perform this type of studies, conversion should be kept low, therefore a reduction of reaction temperature or an increase of the flow rate in comparison to the conditions used on this work must be performed.

It is proposed a change on the setup. Indeed, with some investment, this experimental setup could hold three different columns at the same time, but because this experiments took so much time, this change will improve the quantity of results that is possible to obtain when one is doing catalyst screening or even kinetics with different catalysts and also save electricity.

Also due to the extensive time that was needed and in order to save the reactants consumption, it is proposed the determination of the kinetics not by continuous flow in this fixed-bed reactor but modifying it with a continuous recycling to simulate a batch reactor. If it works, will save considerable amounts of reactants.

Finally, zeolites are famous by their microporous character, but this very microporous structure hinders the molecular transport of reactant to access the active acid sites. Many studies have been performed to solve this limitation, most of them try to alter the porous structure by either direct synthesis or post-synthesis treatment, which is called zeolite modification. Various approaches have been taken: creation of large cavities, nanocrystals and delamination, but one

of the most important is the formation of mesopores in zeolite crystals. In this work, mordenite samples had higher mesoporosity than beta and yielded higher conversions than the latter, which is was assumed by the facilitated transport of molecules inside the mesoporous network. Additionally, MOR-40 has a bimodal pore distribution, with one peak in the range of mesopores that seems to improve xylene conversion.

It is proposed the study of mesoporous formation by techniques like carbon templating, desilication, and dealumination. The latter is a widely explored field, but the problem with removing the aluminum content is the impact on the Bronsted acids amount, especially for some catalyst like MFI that are very siliceous zeolites and have low concentration of aluminum, therefore it will be difficult to induce some mesoporosity by aluminum removal. However, the removal of silicium, desilication, does not change significantly the acids amount. These studies are very valuable, because a small improvement on catalyst selectivity and activity will give major profits for industry, when one is considering the total annual production time.

6.3 Final Assessment

This dissertation helped me to consolidate the knowledge of this area, acid heterogeneous catalysis, acquired during the Reaction Engineering III course. Furthermore, the healthy relationship with all LSRE associates helped me to develop a more pragmatic and scientific spirit inside the laboratory and even improve my skills in basic software like Word and Excel.

Even if the primary objective of this thesis was changed due to lack of time, the balance is very positive.

7 References

1. Meyers, R., *Handbook of petroleum refining processes* 2004: McGraw-Hill.
2. Ltd.), M.R.F.P.o.W.R.A.M.P. *Global Para Xylene Market Research Report- Forecast to 2022*. 2018 [cited 2019 4th of february]; Available from: <https://www.marketresearchfuture.com/reports/para-xylene-market-2278>.
3. Gonçalves, J.C. and A.E. Rodrigues, *Simulated moving bed reactor for p-xylene production: Adsorbent and catalyst homogeneous mixture*. *Chemical Engineering Journal*, 2014. **258**: p. 194-202.
4. Lv, J., et al., *Surface-Passivated Hierarchically Structured ZSM5 Zeolites: High-Performance Shape-Selective Catalysts for para-Xylene Production*. *ChemCatChem*, 2018. **10**(10): p. 2278-2284.
5. Keith A Couch and Claudio Bertelli, U.A.H.C., *Seizing Opportunity*, in *Hydrocarbon Engineering*. 2015.
6. Peng, H., et al., *9 - Flexible Electronic Devices Based on Polymers*, in *Polymer Materials for Energy and Electronic Applications*, H. Peng, et al., Editors. 2017, Academic Press. p. 325-354.
7. Turton, R., R. C. Bailie, and W. Whiting, *Analysis, synthesis and design of chemical processes*. 2003.
8. Aransiola, E., M.O. Daramola, and T. Ojumu, *Xylenes: Production technologies and uses*. 2013. 1-12.
9. Wantanachaisaeng, P. and K. O'Neil, *Capturing opportunities for para-xylene production*. Vol. 17. 2007. 38-45.
10. Aitani, A., *Catalytic Naphtha Reforming*. 2006. p. 12-397.
11. Dawagreh, A.K., S. Chand, and I. Mishra, *Disproportionation of Toluene to Produce Benzene and p- Xylene - A Review*. Vol. 60. 2001. 319-327.
12. Yang, Y., P. Bai, and X. Guo, *Separation of Xylene Isomers: A Review of Recent Advances in Materials*. *Industrial & Engineering Chemistry Research*, 2017. **56**(50): p. 14725-14753.
13. Rowe, C.N. and R.W. Schiessler, *Adsorption Separation Factors and Selective Adsorbent Capacities of Some Binary Liquid Hydrocarbon Mixtures*¹. *The Journal of Physical Chemistry*, 1966. **70**(3): p. 787-797.
14. Krishna, R., *Separating mixtures by exploiting molecular packing effects in microporous materials*. *Physical Chemistry Chemical Physics*, 2015. **17**(1): p. 39-59.
15. Gonçalves, J.C., A.F.P. Ferreira, and A.E. Rodrigues, *Minimum Cross Diameter for C6-C10 Aromatic Compounds*. *Chemical Engineering & Technology*, 2019. **42**(5): p. 1169-1173.
16. Stankiewicz, A. and J.A. Moulijn, *Process Intensification: Transforming Chemical Engineering*. Vol. 96. 2000. 22-33.
17. Rodrigues, A.E., et al., *Chapter 8 - Simulated Moving Bed Reactor*, in *Simulated Moving Bed Technology*, A.E. Rodrigues, et al., Editors. 2015, Butterworth-Heinemann: Oxford. p. 183-223.

18. Minceva, M., et al., *Simulated moving bed reactor for isomerization and separation of p-xylene*. Vol. 140. 2008. 305-323.
19. Shi, Q., et al., *Xylene Isomerization over Beta Zeolites in Liquid Phase*. Industrial & Engineering Chemistry Research, 2018. **57**(16): p. 5568-5579.
20. Cappellazzo, O., et al., *Kinetics of shape-selective xylene isomerization over a ZSM-5 catalyst*. Industrial & Engineering Chemistry Research, 1991. **30**(10): p. 2280-2287.
21. Guisnet, M., N. Gnep, and S. Morin, *Mechanisms of Xylene Isomerization over Acidic Solid Catalysts*. Vol. 35-6. 2000. 47-59.
22. Byun, Y., et al., *Theoretical Investigation of the Isomerization and Disproportionation of m-Xylene over Medium-Pore Zeolites with Different Framework Topologies*. ACS Catalysis, 2014. **4**(6): p. 1764-1776.
23. Gonçalves, J.C. and A.E. Rodrigues, *Industrial Xylene/Ethylbenzene Isomerization Unit Using a Radial-Flow Reactor and EUO-Type Zeolite*. Chemical Engineering & Technology, 2013. **36**(10): p. 1658-1664.
24. Shi, Q., et al., *Xylene isomerization side reactions over Beta zeolite: Disproportionation and transalkylation of C8 aromatics and toluene*. Applied Catalysis A: General, 2018. **562**: p. 198-205.
25. L. Hanson, K. and A. J. Engel, *Kinetics of Xylene Isomerization Over Silica-Alumina Catalyst*. Vol. 13. 1967. 260-266.
26. Sie Neftehim, L. *Xylene Isomerization*. [cited 2019 20/5]; Available from: <http://neftchim.com/manual/xylene-isomerization/>.
27. Gendy, T., *Isomerization of ortho-xylene over hydrogen Y zeolite catalyst*. 2019.
28. Chester, A.W. and E.G. Derouane, *Zeolite Characterization and Catalysis*. 2009: Springer Science & Business Media.
29. Mohau Moshoeshe, M.S.N.-T., Veronica Obuseng, *A Review of the Chemistry, Structure, Properties and Applications of Zeolites*. American Journal of Materials Science, 2017. **7**.
30. *Zeolites and Other Micro- and Mesoporous Molecular Sieves*, in *Kirk-Othmer Encyclopedia of Chemical Technology*.
31. Ribeiro, F.R., et al., *Structure-activity relationship in zeolites*. Journal of Molecular Catalysis A: Chemical, 1995. **96**(3): p. 245-270.
32. K. Beyer, H., *Dealumination Techniques for Zeolites*. 2002. p. 203-255.
33. Bauer, F., E. Bilz, and A. Freyer, *Selectivity improvement in xylene isomerization*. Vol. 154. 2004. 2169-2178.
34. Poursaeidesfahani, A., et al., *Product shape selectivity of MFI-type, MEL-type, and BEA-type zeolites in the catalytic hydroconversion of heptane*. Journal of Catalysis, 2017. **353**: p. 54-62.
35. Smit, B. and J. Ilja Siepmann, *Simulating Adsorption of Alkanes in Zeolites*. Science (New York, N.Y.), 1994. **264**: p. 1118-20.
36. Jacobs, P.A. and J.A. Martens, *Chapter I: Synthesis of ZSM-5 Zeolites in the Presence of Tetrapropylammonium Ions*, in *Studies in Surface Science and Catalysis*. 1987, Elsevier. p. 47-111.
37. González, M.D., Y. Cesteros, and P. Salagre, *Comparison of dealumination of zeolites beta, mordenite and ZSM-5 by treatment with acid under microwave irradiation*. Microporous and Mesoporous Materials, 2011. **144**(1): p. 162-170.

38. Aly, H.M., M.E. Moustafa, and E.A. Abdelrahman, *Synthesis of mordenite zeolite in absence of organic template*. Advanced Powder Technology, 2012. **23**(6): p. 757-760.
39. Degnan, T.F., C.M. Smith, and C.R. Venkat, *Alkylation of aromatics with ethylene and propylene: recent developments in commercial processes*. Applied Catalysis A: General, 2001. **221**(1): p. 283-294.
40. Ch. Baerlocher, L.B.M. *Database of Zeolite Structures*. 2017 [cited 2019 7th of August]; Available from: <http://www.iza-structure.org/databases/>.
41. Bejblová, M., N. Žilková, and J. Čejka, *Transformations of aromatic hydrocarbons over zeolites*. Vol. 34. 2008. 439-454.
42. Gonçalves, J.C. and A.E. Rodrigues, *Xylene Isomerization in the Liquid Phase Using Large-Pore Zeolites*. Chemical Engineering & Technology, 2016. **39**(2): p. 225-232.
43. Akhtar, F., et al., *Structuring adsorbents and catalysts by processing of porous powders*. Journal of the European Ceramic Society, 2014. **34**(7): p. 1643-1666.
44. Miyamoto, Y., N. Katada, and M. Niwa, *Acidity of B zeolite with different Si/Al₂ ratio as measured by temperature programmed desorption of ammonia*. Microporous and Mesoporous Materials, 2000. **40**(1): p. 271-281.
45. Ng, E.-P. and S. Mintova, *Nanoporous materials with enhanced hydrophilicity and high water sorption capacity*. Microporous and Mesoporous Materials, 2008. **114**(1): p. 1-26.
46. Csicsery, S.M., *Shape-selective catalysis in zeolites*. Zeolites, 1984. **4**(3): p. 202-213.
47. Guisnet, M. and P. Magnoux, *Coking and deactivation of zeolites: Influence of the Pore Structure*. Applied Catalysis, 1989. **54**(1): p. 1-27.
48. Silva, J.M., et al., *Transformation of an ethylbenzene-o-xylene mixture on HMOR and Pt-HMOR catalysts. Comparison with ZSM-5 catalysts*. Applied Catalysis A: General, 1995. **125**(1): p. 15-27.
49. P. Bolton, A., M. A. Lanewala, and P. E. Pickert, *Isomerization of the diethylbenzenes using zeolite catalysts*. Vol. 33. 1968.
50. Aguayo, A.T., et al., *Regeneration of a HZSM-5 zeolite catalyst deactivated in the transformation of aqueous ethanol into hydrocarbons*. Catalysis Today, 2005. **107-108**: p. 410-416.

Appendix A - Regeneration Program

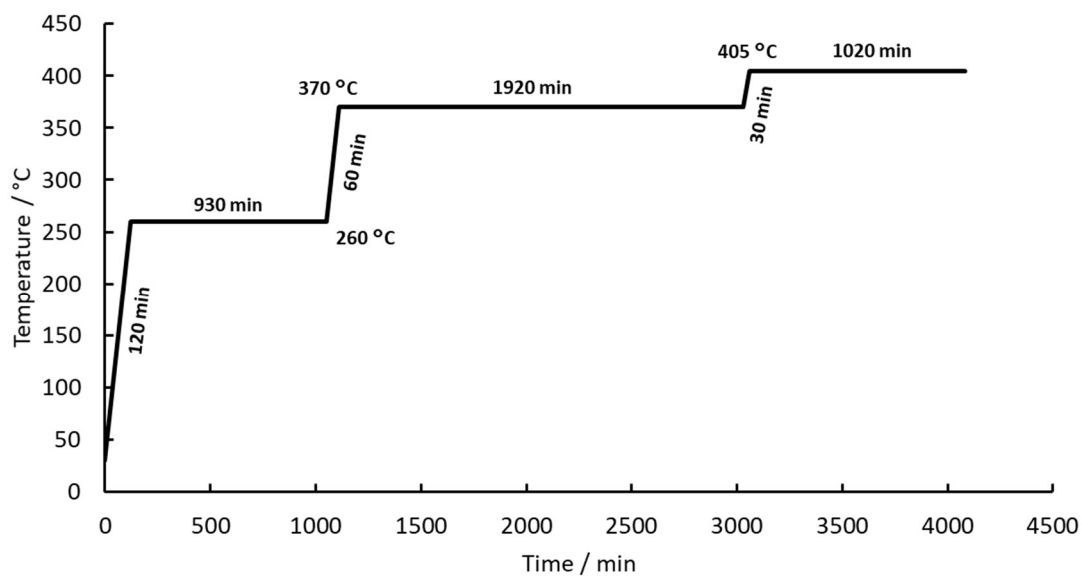


Figure A1. Regeneration Temperature Program

Appendix B - Chromatographs

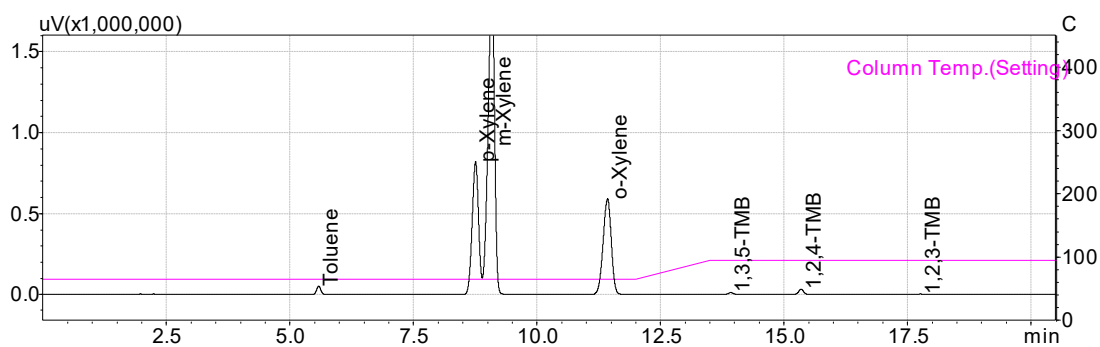


Figure B2. Chromatogram of a normal isomerization method, where the slowest compounds are TMBs.

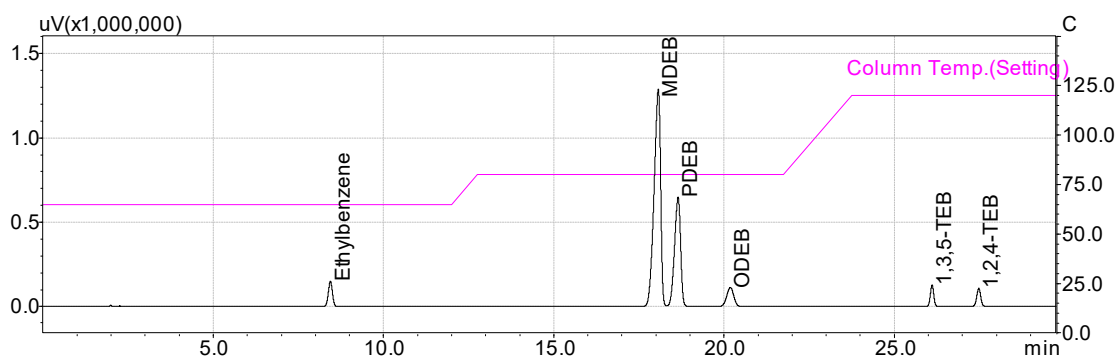


Figure B3. Chromatogram of side reactions method, where the slowest compounds are TEBs.

Appendix C - SEM

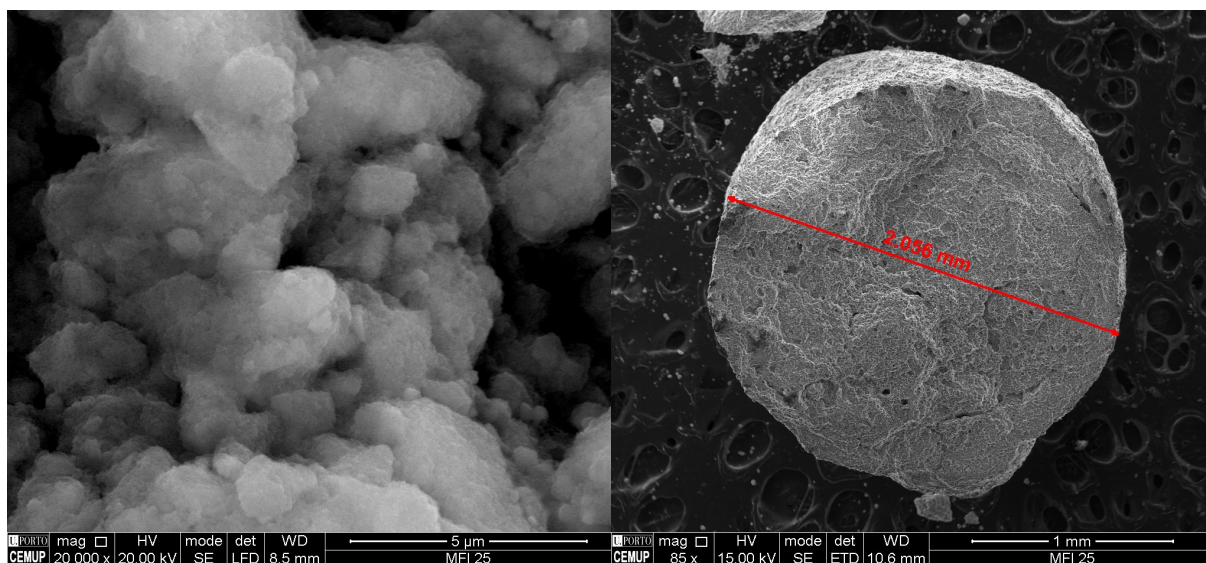


Figure C1. SEM images for MFI-25.

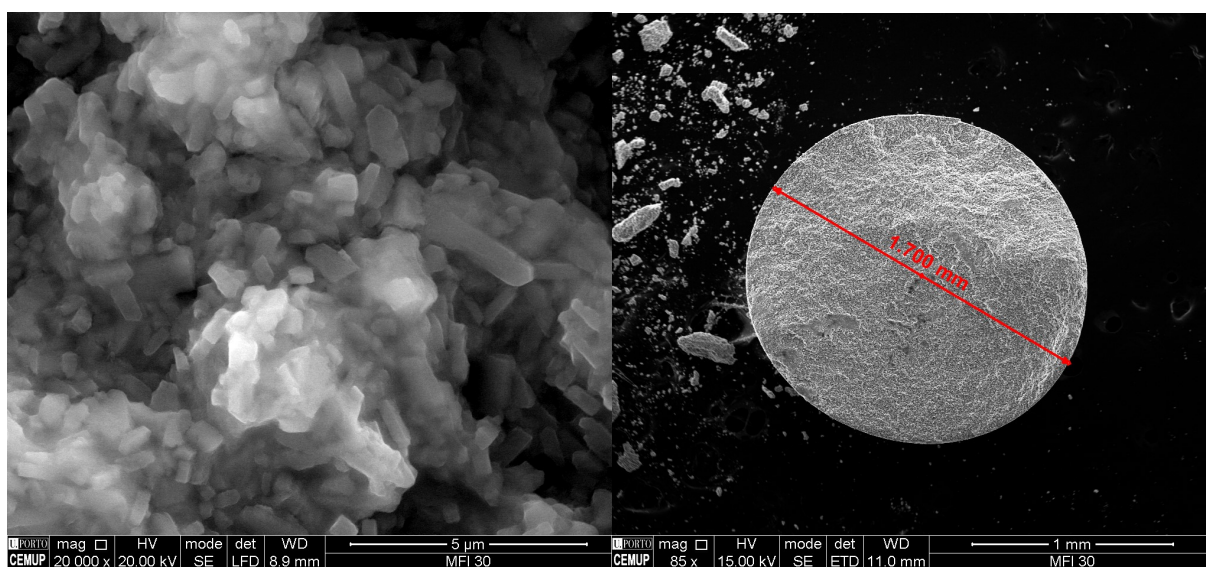


Figure C2. SEM images for MFI-30.

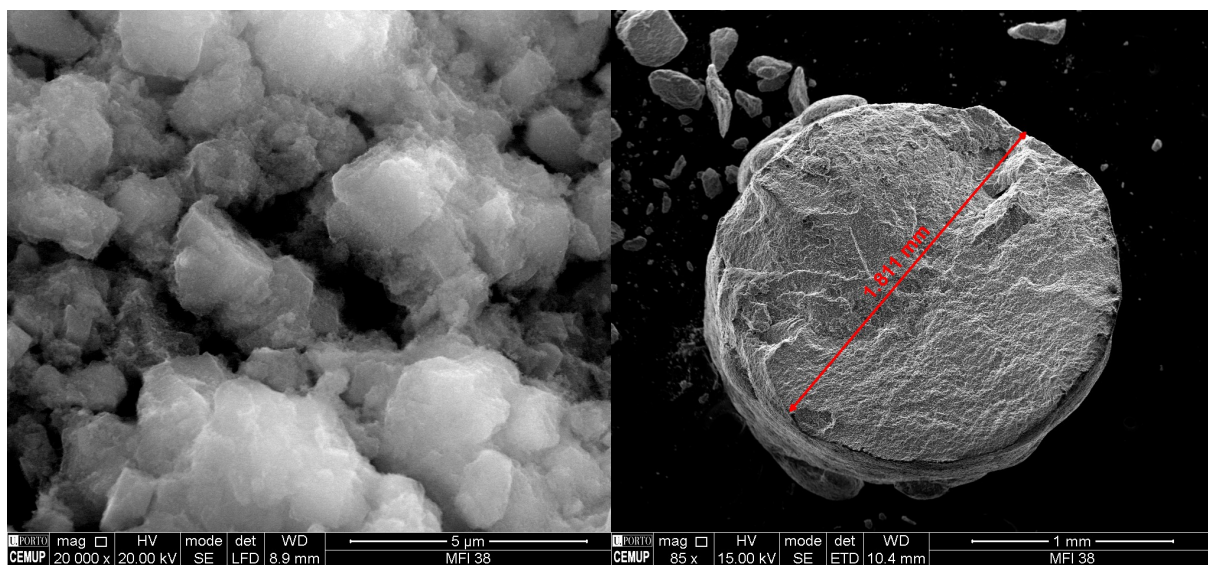


Figure C3. SEM results for MFI-38

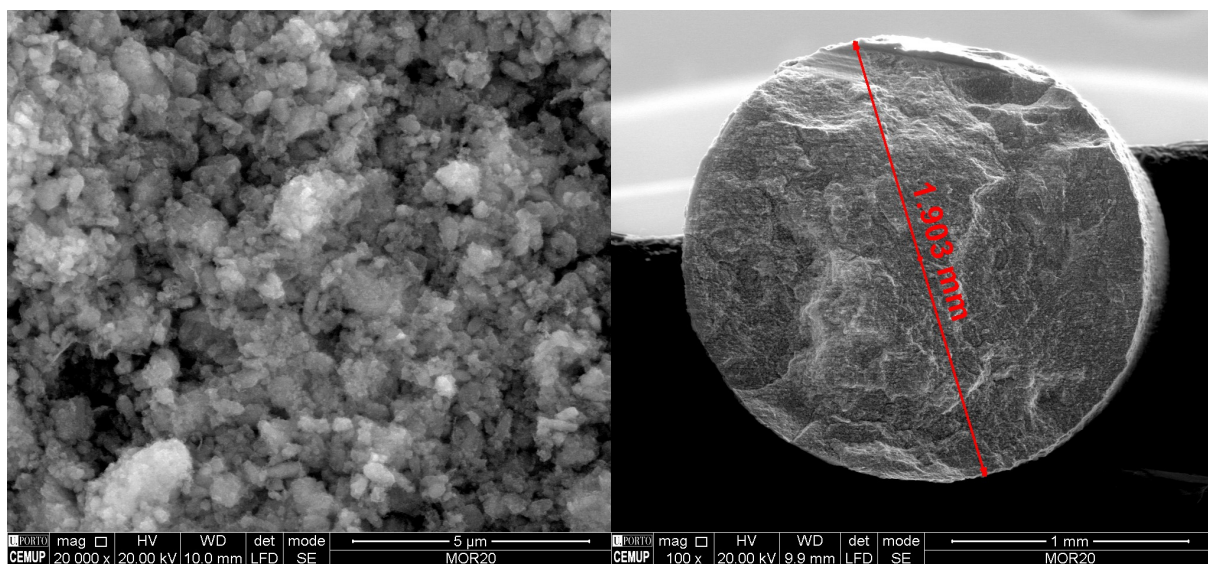


Figure C4. SEM images for MOR-20.

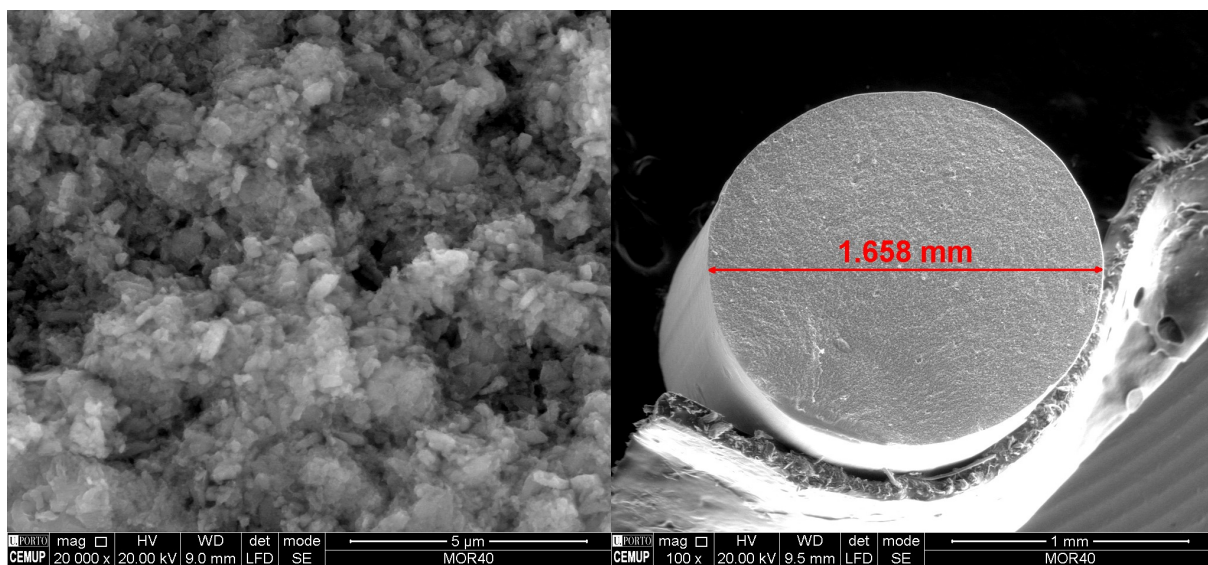


Figure C5. SEM images for MOR-40.

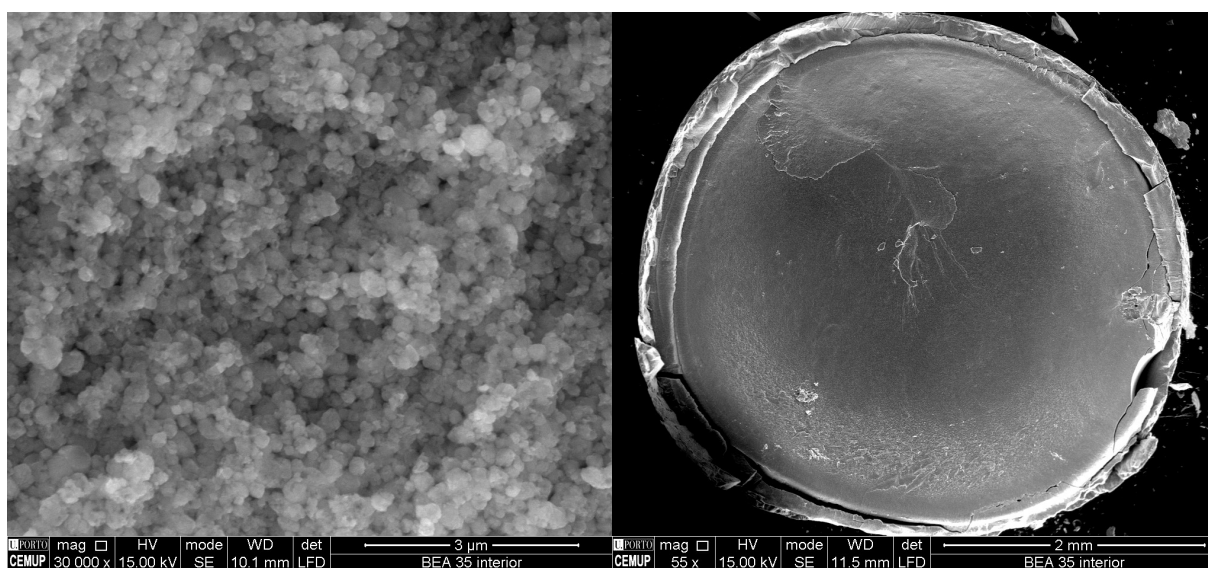


Figure C6. SEM images for BEA-35.

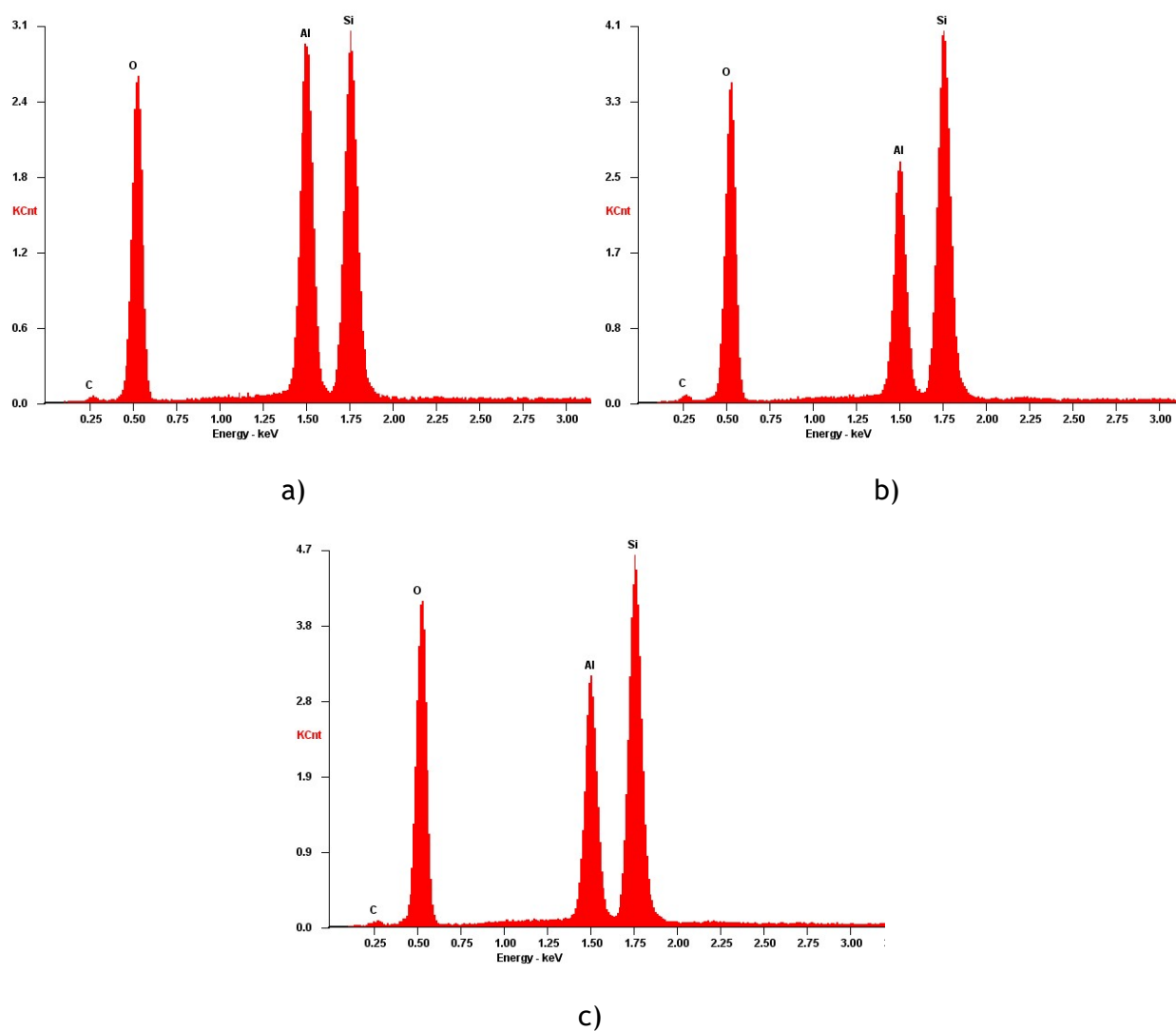


Figure C7. EDS results for a) MFI-25, b) MFI-30, c) MFI-38.

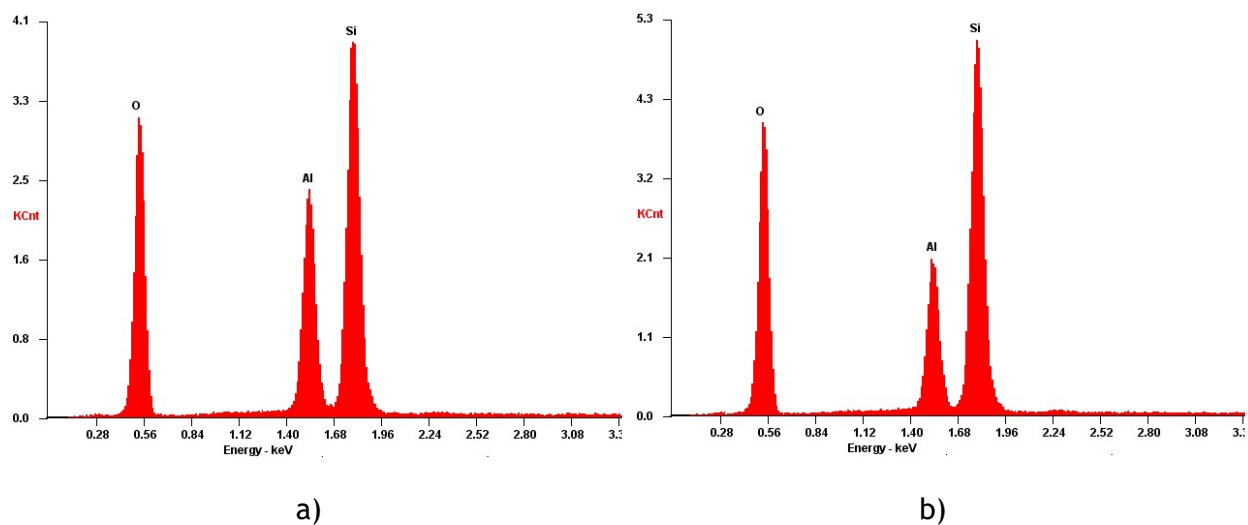


Figure C8. EDS results for a) MOR-20, b) MOR-40.

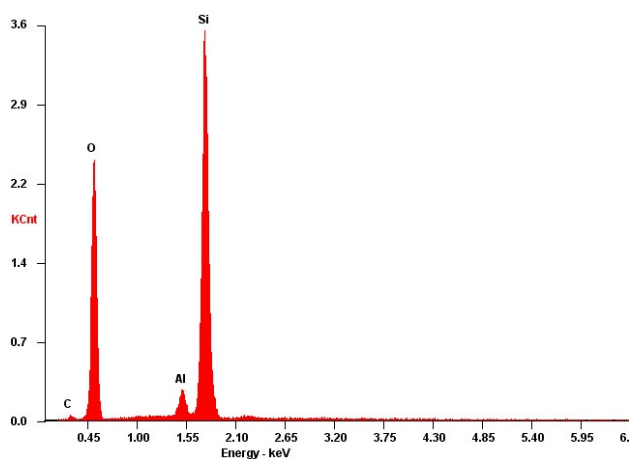


Figure C9. EDS results for BEA-35. Notice that the small amount of aluminium is due to the fact that this zeolite was shaped without addition of binder.

Appendix D - Mass transfer resistances

Mass transfer resistances affect reaction rate and are highly influenced by flow conditions, temperature, and pressure in the reactor. These resistances are due to the difficulty of reactant molecules to diffuse through either the fluid layer (external resistance) or through the very particle pore (internal resistance) [1].

Therefore, to approach any kinetics measurement or to compare the conversions between the catalyst, it is important to understand if mass transfer resistances have an actual effect on obtained conversion.

Criteria to determine the influence of external and internal resistances is calculated in order to see if there is an acceptable deviation from the actual intrinsic rate. If this deviation is very small, then one can neglect the effect of these resistances. To analyze the absence of extraparticle mass transfer, Carberry number criteria can be used, while for intraparticle mass transfer Weisz-Prater is used [2].

External Mass Resistance

Carberry Number (Ca) was calculated by Equation D.1 and it is the quotient between the observed rate and the bulk mass transport rate, therefore if $Ca < 0.05$, external mass resistances can be neglected [1].

$$Ca = \frac{R_{obs}\rho_p \frac{V_p}{S_p}}{k_f C_b} \quad (D.1)$$

ρ_p , V_p , S_p are respectively the density, the volume, and the area of the particle; k_f is the liquid to solid mass transport coefficient and C_b is the bulk concentration.

In order to calculate k_f , Wilson and Geankoplis correlation, Equation D.2, was used, which is valid for $ReSc \gg 1$ [2, 9].

$$Sh = \frac{1.09}{\varepsilon} (ReSc)^{0.33} \quad (D.2)$$

where Sherwood number (Sh) is defined by the quotient of k_f and characteristic dimension (L) by the mass diffusivity (D_m), Equation D.3. As described in Equation D.4, Schmidt number (Sc) is the quotient of kinetic viscosity of the fluid by the product of its density (ρ) and D_m . Reynolds number (Re) is defined by the Equation D.5, where v is the superficial velocity and d_p is the particle diameter [2, 9].

$$\text{Sh} = \frac{k_f}{D_m/L} \quad (\text{D.3})$$

$$\text{Sc} = \frac{\mu}{\rho D_m} \quad (\text{D.4})$$

$$\text{Re} = \frac{\rho v d_p}{\mu} \quad (\text{D.5})$$

To estimate the mass diffusivity two equations were used: Wike-Chang, Equation D.6, and self-diffusivity proposed by Bird, Equation D.8 [2, 3].

$$D_{i,m} = 7.4 \times 10^{-8} \frac{T(\Phi M)^{0.5}}{\mu_m V_i^{0.6}} \quad (\text{D.6})$$

$$\Phi M = \sum_{\substack{j=1 \\ j \neq i}} x_j \Phi_j M_j \quad (\text{D.7})$$

where M is the molecular weight of a solute, Φ is the association coefficient, that is dependent of the solvent and in this case equal to the unity, and x the solute fraction [3].

Equation D.8 is used for self-diffusion coefficient (D_{AA}) estimation, for binary liquid mixtures at infinite dilution where solute A and solvent B are identical. Diffusion admits that there is a concentration gradient, which may not be exactly the case, for example, when reaction is the limiting step. Additionally, is important to notice that in a mixture of solute A in a solvent B, infinite dilution means almost pure B, but for engineering proposes is normal to assume a concentration of A between 5 to 10 mol % [3].

$$\frac{D_{AA} \mu_A}{KT} = \frac{1}{2\pi} \left(\frac{N}{\tilde{V}_A} \right)^{1/3} \quad (\text{D.8})$$

where K is the Boltzmann constant, N is the Avogadro number and \tilde{V} is the molar volume of the liquid at temperature T .

Yamada and Gunn (1973) correlation was used to calculate the liquid molar volume at reaction temperature and at normal boiling point, Equation D.9 [3].

$$V = V_c (0.29056 - 0.08775\omega)^{(1-T/T_c)^{2/7}} \quad (\text{D.9})$$

where V_c is the critical volume, ω the acentric factor and T_c critical temperature.

The final results for external mass-transfer resistance are represented in Table D.1 for all MX experiments and in Table D.2 for PDEB experiments, which state that there is not any external resistance.

Table D.1. Evaluation of external mass resistance for MX experiments.

	Robs x10⁷ (mol g _{cat} ⁻¹ s ⁻¹)	Re	D_m x10⁵ (cm ² s ⁻¹)	K_f (cm s ⁻¹)	Ca x10⁵
MFI-25	2.61	1.5	13.84	0.034	3.65
MFI-30	2.81	1.2	13.84	0.032	3.38
MFI-38	1.09	1.4	13.84	0.037	1.40
MOR-20	23.47	1.4	9.41	0.023	40.44
MOR-40	28.03	1.2	10.76	0.042	20.83
BEA-35	17.89	2.3	8.91	0.019	62.05

Table D.2. Evaluation of external mass resistance for PDEB experiments.

	Robs x10⁶ (mol g _{cat} ⁻¹ s ⁻¹)	Re	D_m x10⁵ (cm ² s ⁻¹)	K_f (cm s ⁻¹)	Ca x10⁵
MFI-25	1.47	1.2	6.75	0.021	0.00
MOR-20	3.87	1.3	10.29	0.029	0.00

Internal Mass resistances

To evaluate the significance of internal mass-transfer resistances, Weisz-Prater method was used, Equation D.10 [5]. This equation is valid for first order systems with irreversible reactions, therefore the conversion must be kept as low as possible. If $\eta\phi^2 \ll 1$ no pore diffusion limitation is present. Extra attention should be given when treating high conversion results for example of MOR-20, MOR-40 and BEA-35 with Equation D.10, because at this concentrations this reactions can be reversible, but because this is not a kinetic study, it is admissible to use it just to have an idea of how far the samples are from being limited by reaction rate.

$$\eta\phi^2 = \frac{R_{obs}(V_p/S_p)^2}{D_e C_s} \quad (D.10)$$

where C_s is the surface concentration of the particle and D_e is effective diffusivity, which was calculated by equation D.11 with assumption that tortuosity factor (τ) is equal to the inverse of the square root of porosity (ϵ) [5].

$$D_e = D_m \epsilon^{1.5} \quad (D.11)$$

It is known that there are many types of diffusion. In macropores, the pore size is bigger than the molecules free path (molecular diffusion), but in the crystals is very situational, for example MFI pore size is very close to the free path of the molecule, so it moves by continuously touching the solid (configurational diffusion) [6].

Very often, in kinetics studies, all the diffusional resistances are lumped into the reaction constants, due to high difficulty to have a precise quantification of them individually [7].

The product $\eta\phi^2$ was also calculated using the theoretical equations obtained for each catalyst geometry in order to get the Thiele modulus (ϕ) and effectiveness factor (η) [6].

$$\text{slab} \quad \eta\phi^2 = \phi \tanh(\phi) \quad (\text{D.12})$$

$$\text{Semi-infinite cylinder} \quad \eta\phi^2 = \phi \frac{I_1(2\phi)}{I_2(2\phi)} \quad (\text{D.13})$$

$$\text{sphere} \quad \eta\phi^2 = \phi \left(\frac{1}{\tanh(3\phi)} - \frac{1}{3\phi} \right) \quad (\text{D.14})$$

The results for internal mass transfer, Table D.3 and table D.4, show that they are negligible.

Table D.3. Evaluation of internal mass transfer resistances for MX experiments.

	$D_e \times 10^5$ ($\text{cm}^2 \text{ s}^{-1}$)	$\eta\phi^2 \times 10^4$	Cylinder		Sphere		Slab	
			ϕ	η	ϕ	η	ϕ	η
MFI-25	4.32	9.61	0.03	1.00	0.03	1.00	0.03	1.00
MFI-30	4.60	6.60	0.03	1.00	0.03	1.00	0.03	1.00
MFI-38	3.50	4.53	0.02	1.00	0.02	1.00	0.02	1.00
MOR-20	3.23	141.02	0.12	1.00	0.12	0.99	0.12	0.99
MOR-40	2.93	146.07	0.12	1.00	0.12	0.99	0.12	0.99
BEA-35	1.39	602.62	0.25	0.98	0.25	0.96	0.25	0.97

Table D.4. Evaluation of internal mass transfer resistances for PDEB experiments.

	$D_e \times 10^5$ ($\text{cm}^2 \text{ s}^{-1}$)	$\eta\phi^2 \times 10^2$	Cylinder		Sphere		Slab	
			ϕ	η	ϕ	η	ϕ	η
MFI-25	2.11	1.96	0.14	0.99	0.14	0.99	0.14	0.99
MOR-20	3.21	7.08	0.27	0.98	0.27	0.96	0.27	0.97

Compound properties

All physical properties and correlation parameters were taken from Yaws and are listed on table X and Y [8].

The mixture was assumed ideal in order to calculate the viscosity and density using pure compound values for these properties. Grunberg and Nissan's method was used to estimate viscosity and density was calculated by weighted average density [3].

$$\mu_{mixture} = \prod_j \mu_j^{x_j} \quad (D.15)$$

$$\rho = \frac{M}{\sum_j \frac{V_j}{x_j}} \quad (D.16)$$

Table D.5. Physical and critical properties of compounds of interest [8].

	molar mass g·mol ⁻¹	P _c bar	T _c K	T _b K	ω	V _c cm ³ ·mol ⁻¹	V _{Tb} cm ³ ·mol ⁻¹	V _{240 K} cm ³ ·mol ⁻¹
OX	106.167	37.34	630.37	417.58	0.313	369.2	138.7	161.6
MX	106.167	35.41	617.05	412.27	0.326	375.8	141.4	167.9
PX	106.167	35.11	616.26	411.51	0.326	379.1	142.6	169.6
Bz	78.11	48.98	562.16	353.24	0.211	258.9	97.1	135.3
EB	106.167	36.09	617.17	409.35	0.304	373.8	140.8	167.7
Tol	92.14	41.09	591.79	383.78	0.264	315.8	118.7	150.5
1,2,4-TMB	120.19	32.32	649.13	442.53	0.379	430.0	161.6	180.4
1,2,3-TMB	120.19	34.54	664.53	449.27	0.366	414.0	155.3	170.5
1,3,5-TEB	162.275	23.36	682.28	489.16	0.479	599.5	227.1	235.4
1,2,4-TEB	162.275	23.36	684.37	490.66	0.479	599.5	227.1	234.8
ODEB	134.221	28.80	668.00	456.61	0.340	502.0	190.7	207.1
MDEB	134.221	28.80	663.00	454.29	0.350	488.0	185.2	202.1
PDEB	134.221	28.03	657.96	456.94	0.404	497.0	187.7	204.8
Heptane	100.21	27.36	540.26	371.58	0.351	431.9	164.3	243.2

Table D.6. Parameters of liquid density correlation for compounds of interest [8].

	$\rho = A \times B^{-\left(1-\frac{T}{T_c}\right)^N}$				Pure compound ρ in g·cm ⁻³ at 513 K
	density ρ in g·cm ⁻³ , T in K				
	A	B	N	TC	
OX	0.2838	0.2608	0.2741	630.37	0.663
MX	0.2787	0.2593	0.2724	617.05	0.640
PX	0.2798	0.2600	0.2790	616.26	0.634
Bz	0.3009	0.2677	0.2818	562.16	0.584
EB	0.2889	0.2644	0.2921	617.17	0.637
Tol	0.3000	0.2711	0.2989	591.79	0.613
1,2,4-TMB	0.2797	0.2595	0.2772	649.13	0.671
1,2,3-TMB	0.2906	0.2703	0.2608	664.53	0.707
1,3,5-TEB	0.2707	0.2470	0.2857	682.28	0.692
1,2,4-TEB	0.2644	0.2460	0.2857	684.37	0.680
ODEB	0.2747	0.2534	0.2857	668.00	0.679
MDEB	0.2733	0.2566	0.2857	663.00	0.665
PDEB	0.2708	0.2540	0.2857	657.96	0.659
Heptane	0.2324	0.2602	0.2791	540.26	0.417

Table D.7. Parameters of viscosity correlation for compounds of interest [8].

	$\mu = 10^{A + \frac{B}{T} + C \times T + D \times T^2}$				Pure compound μ in cP at 513 K
	Viscosity μ in cP, T in K				
	A	B	C	Dx10 ⁵	
OX	-7.8805	1250.0	0.0161	-1.399	0.136
MX	-6.0517	924.6	0.0126	-1.185	0.125
PX	-9.4655	1440	0.0199	-1.699	0.120
Bz	-7.4005	1181.5	0.0149	-1.371	0.087
EB	-5.2585	830.7	0.0108	-1.062	0.128
Tol	-5.1649	810.7	0.0105	-1.049	0.110
1,2,4-TMB	-8.4686	1361.7	0.0173	-1.461	0.164
1,2,3-TMB	-14.3160	2225.6	0.0295	-2.250	0.171
1,3,5-TEB	-7.4921	1324.7	0.0143	-1.192	0.194
1,2,4-TEB	-7.4748	1326.0	0.0142	-1.183	0.191
ODEB	-7.1296	1220.4	0.0136	-1.153	0.156
MDEB	-7.2924	1235.1	0.0141	-1.199E	0.156
PDEB	-7.6851	1286.2	0.0152	-1.296	0.161
Heptane	-5.7782	805.87	0.0134	-1.479	0.059

Appendix E - EB/Tol Experiments

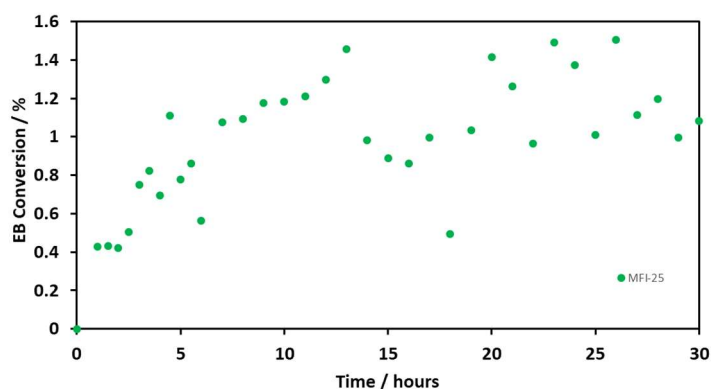


Figure E.1. Ethylbenzene conversion as function of time for MFI-25.

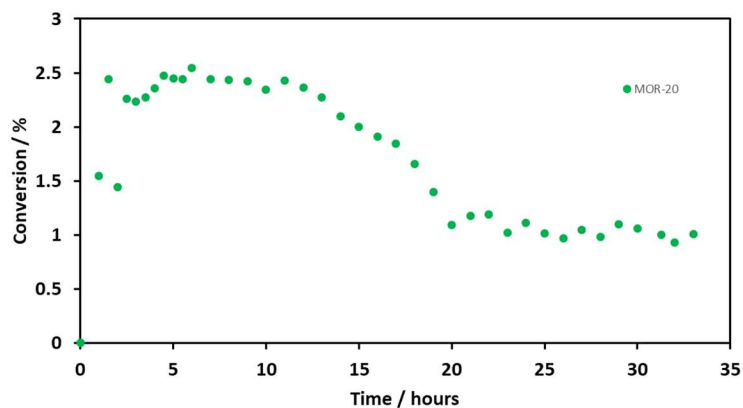


Figure E.2. Ethylbenzene conversion as function of time for MOR-20.

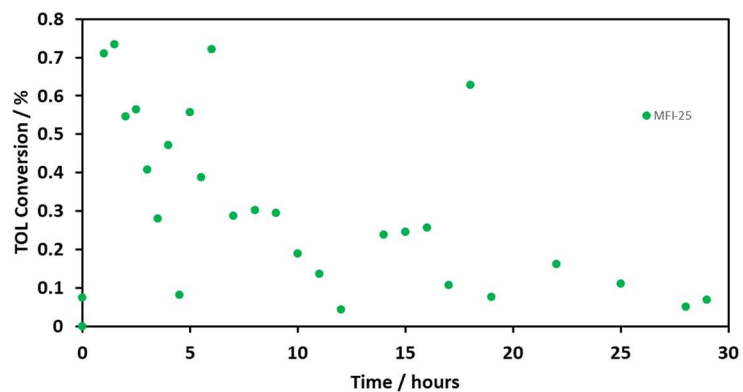


Figure E.3. Toluene conversion as function of time for MFI-25.

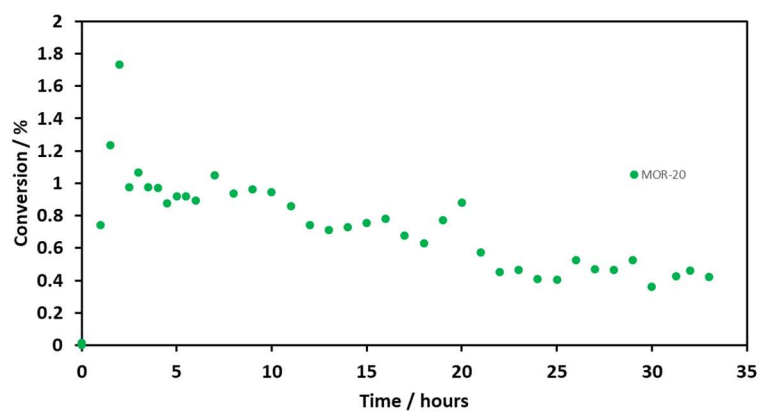


Figure E.4. Toluene conversion as function of time for MOR-20.

Appendix References

1. Fogler, H.S., *Elements of chemical reaction engineering*. 1999: Third edition. Upper Saddle River, N.J. : Prentice Hall PTR, [1999] ©1999
2. Dekker, F.H.M., *et al.*, *Analysis of mass and heat transfer in transient experiments over heterogeneous catalysts*. *Chemical Engineering Science*, 1995. 50(22): p. 3573-3580.
3. Bird, R.B., W.E. Stewart, and E.N. Lightfoot, *Transport Phenomena*. 2006: Wiley
4. Poling, B.E., J.M. Prausnitz, and J.P. O'Connell, *The Properties of Gases and Liquids* 5E. 2000: McGraw-Hill Education.
5. Levenspiel, O., *Chemical reaction engineering*. 1999: Wiley.
6. Pisani, L., *Simple Expression for the Tortuosity of Porous Media*. *Transport in Porous Media*, 2011. 88(2): p. 193-203.
7. Chang, X., Y. Li, and Z. Zeng, *Kinetics study of the isomerization of xylene on HZSM-5 zeolite. 1. Kinetics model and reaction mechanism*. *Industrial & Engineering Chemistry Research*, 1992. 31(1): p. 187-192.
8. Yaws, C.L., *Yaws' Handbook of Thermodynamic and Physical Properties of Chemical Compounds*. Knovel.
9. Ruthven, D.M., *Principles of adsorption and adsorption processes*. First ed. 1985, Chichester: Wiley and Sons Ltd.